SLAC-PUB-5267
July 1991
(A/T)

LONG-TERM BOUNDS ON NONLINEAR HAMILTONIAN MOTION*

R. L. Warnock and R. D. Ruth
Stanford Linear Accelerator Center
Stanford University, Stanford, California 94309

February 1990

ABSTRACT

In various important applications of Hamiltonian mechanics, notably in problems of accelerator design, it would be useful to set bounds on nonlinear motion for finite but very long times. Such bounds can be sought through construction of a canonical transformation to new action-angle variables $(\mathbf{J}, \mathbf{\Psi})$, such that $\mathbf{J}$ is nearly constant, and $\mathbf{\Psi}$ advances almost linearly with the time. By examining the residual change in $\mathbf{J}$ during a time T_o from various initial conditions in the open domain Ω of phase space, one can estimate the change in $\mathbf{J}$ during a much larger time T, on any orbit starting in a smaller open domain $\Omega_o \subset \Omega$. A numerical realization of this idea is described. The canonical transformations, equivalent to close approximations to invariant tori, are constructed by a new method in which surfaces are fitted to computed orbits. The perturbed tunes $\boldsymbol{\nu}$ (winding numbers) are determined as functions of $\mathbf{J}$, and the inverse function $\mathbf{J}(\boldsymbol{\nu})$ is also computed. This leads to an accurate map of resonant tune lines into $\mathbf{J}$ space, which serves to locate dangerous regions of phase space. Near a single strong resonance, $\mathbf{J}$ varies more than usual but follows the pattern expected from the isolated resonance model. All calculations proceed from a time evolution map defined by a symplectic integrator or equivalent explicit formula. As an example, an accelerator problem in 2 1/2 degrees of freedom is treated. For betatron motion in a model accelerator with strong sextupole magnets, stability for 10^8 turns is predicted in a region of substantial nonlinearity.

Submitted to *Physica D*

*Work supported by Departmentof Energy contract DE–AC03–76SF00515.

1. INTRODUCTION

In the design of cyclic particle accelerators and storage rings one encounters generic problems of nonlinear mechanics in several degrees of freedom.[1,2,3] The roles of nonlinear resonances and invariant tori must be analysed, and in many respects the analysis resembles that required in other applications of nonlincar mechanics, especially in topics from celestial mechanics, semi-classical quantum theory, and plasma theory. In other respects the tasks of acccelerator theory are special, and make unusual technical demands. For instance, one must study particles that follow narrowly defined orbits over times that are equivalent to enormous astronomical times. In a modern proton storage ring the protons travel near the velocity of light and are stored for several hours, traveling a total distance of around 10^{13} meters. They interact with nonlinear magnetic fields every few meters. If we regard one interaction as being comparable to one revolution of a planet in the solar system, we see that a proton storage time corresponds to about 10^{12} years of planetary motion!

The usual approach to prediction of long-term stability is based on "tracking", which is direct numerical integration of Hamilton's equations to follow orbits evolving from various initial conditions.[4] Although tracking seems to provide a valuable guide to probable accelerator performance, the time over which an orbit is followed is usually much less than the time desired, and the number of initial conditions that can be tested is severely restricted. These limitations are due to computational expense, and may be gradually reduced through improvements in technique. On the other hand, tracking as practiced has an intrinsic limitation, in that it amounts to blind experimentation, providing little insight about underlying sources of instability.

To approach questions of long-term stability in a more theoretical way, one first considers invariant surfaces in phase space. If the system has d mechanical degrees of freedom, the effective dimension of phase space is $D = 2d + \tau$, where $\tau = 0$ if the system is autonomous and $\tau = 1$ if the Hamiltonian is a periodic function of the time. We are concerned mainly with the latter case, but allow also the former. We exclude non-periodic time dependence of the Hamiltonian. For nearly integrable systems as studied in the Kolmogorov-Arnol'd- Moser (K.A.M.) theory,[5,6] a large set of invariant tori of dimension $d+1$ exists. Under the conditions of the K.A.M. theorem, every invariant torus of the underlying integrable system that has rationally incommensurate frequencies (in the sense of a Diophantine condition) persists under the nonintegrable perturbation. If $D \leq 4$, an invariant torus divides the space into two disjoint regions. We can then predict stability for all time, since if an orbit is inside or on the torus at one time, it must be inside or on the torus at all times. If $D \geq 5$, as is the case in realistic models of storage rings, an invariant torus no longer divides the space so as to confine orbits. Furthermore, arbitrarily close to an invariant torus there are initial conditions for orbits that visit regions of phase space far removed from that torus. Such orbits follow stochastic layers near resonance structures that form a web permeating phase space. This phenomenon is referred to broadly as Arnol'd Diffusion, following the demonstration of such an effect by Arnol'd in an example with $D = 5$. It follows that in high-dimensional systems the existence of invariant surfaces has no direct bearing on stability of orbits in a laboratory experiment, since it would require infinite experimental precision to start an orbit exactly on an invariant surface. We must approach the stability question in a different way, attempting to show that the drift of orbits along resonances is so slow as to be harmless under the conditions of interest. We must seek stability for a finite but very long time.

A mathematical result in this direction was obtained by Nekhoroshev.[7] Stated informally, Nekhoroshev's theorem asserts that any orbit beginning in a certain open domain Ω_o of phase space will be confined to a larger open domain $\Omega \supset \Omega_o$ for a time $t > T$, where T increases exponentially as the strength ϵ of the nonlinear perturbation tends to zero. The Hamiltonian is assumed to be analytic, with a certain "steepness" condition on its unperturbed part. Unfortunately, the theorem has no quantitative significance in problems like those of accelerator design, because ϵ has to be absurdly small to get a stability time T of practical interest. This situation arises from the use of a perturbative argument and the compounding of many pessimistic estimates that are required in the rigorous analysis. Undoubtedly, the true time of stability for a given ϵ is underestimated by a very wide margin.

Various authors have published results of Nekhoroshev type, often modifying the hypotheses so as to give simpler proofs. For instance, the steepness condition has been replaced by a convexity condition,[8] and the case of perturbed harmonic oscillators, a case of interest in accelerator physics, has been treated.[9,10] The study of maps rather than Hamiltonian flows also gives some simplification.[11] Another endeavor is to look for results with parameters closer to realistic magnitudes, by taking advantage of the properties of special Hamiltonians.[12,13] Numerical and heuristic studies of simple models, informed by the work of Arnol'd and Nekhoroshev, have also been carried out.[14]

We wish to show that an argument in the spirit of Nekhoroshev's theorem, but quite different in technique, can be carried out numerically. Without a severe restriction on the strength of the perturbation, we obtain bounds over time intervals of suitable magnitude for accelerator physics. Because of the finite nature of

numerical analysis, the bounds are not mathematically rigorous. Nevertheless, the argument is highly cautious by the standards of theoretical physics, and much more persuasive than the blind extrapolations that are usually used to draw long-term estimates from tracking.

We make a canonical transformation from the action-angle variables $(\mathbf{I}, \mathbf{\Phi})$ of the unperturbed (integrable) system to new action-angle variables $(\mathbf{J}, \mathbf{\Psi})$. In a region of phase-space devoid of low-order resonances of appreciable width, the sort of region preferred for operation of an accelerator, the new action $\mathbf{J}$ is nearly constant, and the new angle $\mathbf{\Psi}$ advances almost linearly with the time. Near a single resonance of substantial width, $\mathbf{J}$ has behavior close to that of the isolated-resonance model. In two degrees of freedom that means that in its time evolution $\mathbf{J}$ closely follows a straight line segment in the (J_1, J_2) plane, the segment being of finite length for stable resonant motion. In other situations, for instance when two broad resonances overlap, $\mathbf{J}$ may have more complicated behavior. The desired "normal" behavior of $\mathbf{J}$ is that it either be nearly constant, or else imitate the motion characteristic of a stable isolated resonance. By looking for deviations of $\mathbf{J}$ from this norm, we acquire a sensitive indicator of undesired behavior. By contrast, the original variable $\mathbf{I}$ typically displays a complicated motion, even when $\mathbf{J}$ behaves normally. Since conventional tracking works with original variables, it fails to reveal a simple normative behavior.

By examining the time variation of $\mathbf{J}$ one can, in principle, derive rigorous long-term bounds on the motion.[15,16,17] Consider an open domain in $\mathbf{J}$ space, say a ball Ω, and suppose that for any orbit with initial action $\mathbf{J}_o$ in Ω the maximum variation of $\|\mathbf{J}\|$ during a time T_o is δJ. Then the action of any orbit with initial action in a smaller ball $\Omega_o \subset \Omega$ cannot leave Ω in a time less than $T = nT_o$,

where $n = \Delta J/\delta J$, and ΔJ is the minimum distance from the boundary of Ω_o to the boundary of Ω. To get the desired large value of n, one has to determine the canonical transformation so that δJ is very small, since the magnitude of ΔJ is usually restricted by experimental conditions (for instance, by the maximum permissible excursion of an accelerator beam).

In attempting to compute δJ numerically, one can sample only a finite number of initial conditions in Ω. Nevertheless, working with a specific example one can make various tests to get a good estimate of the uncertainty due to limited sampling. This uncertainty, which seems rather small in the example that we treat, is the only significant breach of rigor in our argument.

The central task in this program is to find the canonical transformation. As we shall see, this is equivalent to the problem of finding very accurate approximations to invariant tori. We demonstrated in earlier work that such approximations could be constructed by non-perturbative methods.[18,19,20,21,15] Perturbation theory might also be considered, if steps are taken to provide high accuracy through efficient, high-order computations. For instance, the normal-form algorithm of Forest, Berz, and Irwin[22] allows computations of rather high order in accelerator problems. Perturbative programs have also been developed for the purposes of satellite dynamics.[23] For the present work we use a new technique that is less costly and more robust than previous methods.[16,24] The idea is to make a direct fit of toroidal surfaces to orbit points on a Poincaré surface of section, the torus being represented as a Fourier series in angle variables.

The variable $\mathbf{J}$ is defined as the average over Φ of the original action $\mathbf{I}(\mathbf{\Phi})$ on a fitted torus. Only a few tori are fitted, corresponding to a discrete set of values $\mathbf{J} = \mathbf{J_i}$. Tori for all other values of $\mathbf{J}$ are defined by polynomial interpolation in $\mathbf{J}$.

This defines a canonical transformation for all $\mathbf{J}$ in an open region encompassing the $\mathbf{J}_i$. The interpolation forms bridges over resonances, since resonances interleave invariant tori throughout phase space. The canonical transformation is precisely defined, even in the midst of a low-order resonance, and in that respect differs essentially from canonical transformations computed in perturbation theory.

The interpolation in $\mathbf{J}$ is an essential part of our argument, not merely a procedure forced upon us by the use of numerical methods. One could imagine a similar interpolation being used in a purely analytical context. In fact, Pöschel[25] and Chierchia and Gallavotti[26] have proved the existence of smooth interpolations of exact invariant tori in the context of KAM theory. A family of exact tori is parametrized over a Cantor set in frequency space, but can be smoothly embedded in a family of functions parametrized over intervals. Thus, a canonical transformation can be defined in an open region of phase space, in such a way that the new action variable that it defines is a smooth function, strictly constant only on a family of tori parametrized over a Cantor set. This rigorous construction can be viewed as an idealization of our numerical procedure.

All computations in our treatment proceed from the time evolution map that takes a Poincaré surface of section into itself. In the accelerator problem, the phase point of a particle returns to the surface of section after the particle travels N_o turns around the accelerator. In the present report the map is defined by numerical integration of Hamilton's equations with a symplectic integration algorithm.[27] To treat large accelerators economically, it may be desirable to represent the map, or its canonical generator, by an explicit formula that can be evaluated quickly.[28,29]

In Section 2 we establish notation, describe the basic scheme of canonical transformations, and show how to obtain the time evolution map of new variables.

In Section 3 we give the general argument for establishing long-term bounds. In Section 4 we describe the method to approximate invariant tori. Section 5 deals with interpolation procedures and other numerical questions. In Section 6 we give results for a non-trivial example in accelerator theory; namely, motion in two transverse degrees of freedom in a strongly nonlinear sextupole lattice. The Hamiltonian and accelerator parameters are given in Appendix A. Since accelerators are described by a Hamiltonian with periodic time dependence, the phase space of this example is effectively five-dimensional (two momenta, two coordinates, and time). Section 6 deals with a region not containing broad resonances. In Section 7 we demonstrate the special phenomena that occur near a relatively broad resonance. In Section 8 we consider the outlook for further work.

2. TIME-EVOLUTION MAPS AND CANONICAL TRANSFORMATIONS

We deal with a system in d degrees of freedom described by a Hamiltonian of the form

$$H(\mathbf{I}, \mathbf{\Phi}, \theta) = H_o(\mathbf{I}) + V(\mathbf{I}, \mathbf{\Phi}, \theta), \tag{2.1}$$

where the angle θ is the independent variable of Hamilton's equations, which can be the time or a strictly monotonic function of the time. In the general description of a circular accelerator, θ represents azimuthal location on a closed reference orbit. The perturbation V is $2\pi-$periodic in θ:

$$V(\mathbf{I}, \mathbf{\Phi}, \theta + 2\pi) = V(\mathbf{I}, \mathbf{\Phi}, \theta). \tag{2.2}$$

Bold-faced symbols denote $d-$dimensional vectors. The variables $\mathbf{I}, \Phi$ are action-angle variables of the unperturbed system described by $\mathbf{H_o}$.

In Hamilton-Jacobi theory[5,6,18] one seeks a canonical transformation,

$$(\mathbf{I}, \mathbf{\Phi}) \longrightarrow (\mathbf{J}, \mathbf{\Psi}) \quad , \tag{2.3}$$

such that the new action variable $\mathbf{J}$ is constant. The transformation is obtained through a generating function,

$$S(\mathbf{J}, \mathbf{\Phi}, \theta) = \mathbf{J} \cdot \mathbf{\Phi} + G(\mathbf{J}, \mathbf{\Phi}, \theta) \quad , \tag{2.4}$$

where G is $2\pi-$ periodic in θ and in each component of $\mathbf{\Phi}$. Old and new variables are related by nonlinear equations,

$$\mathbf{I} = \mathbf{J} + G_{\mathbf{\Phi}}(\mathbf{J}, \mathbf{\Phi}, \theta) \quad , \tag{2.5}$$

$$\mathbf{\Psi} = \mathbf{\Phi} + G_{\mathbf{J}}(\mathbf{J}, \mathbf{\Phi}, \theta) \quad . \tag{2.6}$$

Subscripts denote partial differentiation. If the generator G satisfies the Hamilton-Jacobi equation, which is the requirement that the new Hamiltonian be independent of $\mathbf{\Phi}$, then by Hamilton's equations

$$\mathbf{J} = \text{constant} \quad , \tag{2.7}$$

and the new angle variable $\mathbf{\Psi}$ advances linearly with θ,

$$\mathbf{\Psi} = \mathbf{\Psi}_o + \boldsymbol{\nu}(\mathbf{J})\theta \quad . \tag{2.8}$$

In accelerator physics, the winding number $\boldsymbol{\nu}(\mathbf{J})$ is called the "tune". The Hamilton-Jacobi equation is

$$H(\mathbf{J} + G_{\boldsymbol{\Phi}}, \boldsymbol{\Phi}, \theta) + G_\theta = H_1(\mathbf{J}, \theta) \quad . \tag{2.9}$$

We are interested in canonical transformations of the form given in (2.5) and (2.6) such that the new variables satisfy the equations (2.7) and (2.8) to a close approximation, but not exactly. Such transformations can be obtained through an iterative numerical solution of the Hamilton-Jacobi equation[18,19,21], but that procedure as implemented to date involves superfluous integrations. For the present work we prefer a method that makes a direct use of the time evolution map on phase space.

We define a Poincaré surface of section in phase space by

$$\theta = 0 \pmod{2\pi N_o} \quad . \tag{2.10}$$

In the case of a cyclic accelerator, θ is a coordinate specifying the azimuthal location of a particle in the machine, equivalent to arc length along a periodic reference orbit (not necessarily circular). In one turn around the machine, the value of θ for a particle increases by 2π. Thus, our surface of section corresponds to a transverse slice through the beam at a fixed location in the laboratory, but we examine values of $(\mathbf{I}, \boldsymbol{\Phi})$ on this slice only after each interval of N_o turns.

The Poincaré return map, which takes the section (2.10) into itself, will be called the "N_o-turn map" and will be denoted as

$$\mathcal{M}(\mathbf{I}, \boldsymbol{\Phi}; N_o) = (\mathbf{I}', \boldsymbol{\Phi}') \quad . \tag{2.11}$$

We are interested in invariant surfaces of this map for $N_o = 1$. Henceforth, the term "invariant tori" will refer to these surfaces. It is convenient to describe the invariant tori by giving $\mathbf{I}$ as a function of $\mathbf{\Phi}$:

$$\mathbf{I} = \mathbf{J} + \mathbf{u}(\mathbf{J}, \mathbf{\Phi}) \quad . \tag{2.12}$$

Here $\mathbf{u}$ is 2π-periodic in each component of $\mathbf{\Phi}$, and has zero mean with respect to $\mathbf{\Phi}$. Thus $\mathbf{J}$ is the average of $\mathbf{I}$:

$$\mathbf{J} = \int_o^{2\pi} \mathbf{I}(\mathbf{J}, \mathbf{\Phi}) d(\mathbf{\Phi}/2\pi) \quad . \tag{2.13}$$

In view of Eq.(2.5) and the periodicity of G in θ and $\mathbf{\Phi}$, we see that $\mathbf{u}$ can be identified with $G_{\mathbf{\Phi}}$ on the surface of section, and that $\mathbf{J}$ in (2.13) is the same as the invariant action defined above. Thus, a value of $\mathbf{J}$ labels each invariant torus, and

$$\mathbf{u}(\mathbf{J}, \mathbf{\Phi}) = G_{\mathbf{\Phi}}(\mathbf{J}, \mathbf{\Phi}, 0) \quad . \tag{2.14}$$

We next consider approximate invariant tori, but retain the same notation. The equation of an approximate invariant torus,

$$\mathbf{I} = \mathbf{J} + \mathbf{u}(\mathbf{J}, \mathbf{\Phi}) \quad , \tag{2.15}$$

may also be regarded as a change of variables,

$$\mathcal{U}(\mathbf{J}, \mathbf{\Phi}) = (\mathbf{I}, \mathbf{\Phi}) \quad . \tag{2.16}$$

The inverse map,

$$\mathcal{U}^{-1}(\mathbf{I}, \mathbf{\Phi}) = (\mathbf{J}, \mathbf{\Phi}) \quad , \tag{2.17}$$

provides a function $\mathbf{J}(\mathbf{I}, \mathbf{\Phi})$ of the original variables that is nearly invariant on orbits of $\mathcal{M}$:

$$\mathbf{J}(\mathbf{I}(\theta), \mathbf{\Phi}(\theta)) \approx \text{constant} \quad , \tag{2.18}$$

$$\theta = 2\pi N_o p, \quad p = 0, 1, 2, \cdots \quad . \tag{2.19}$$

The time evolution of this function, that is to say its deviation from a constant value, will be the object of study in this paper.

The change of variable (2.16) is useful by itself, but it is not a full canonical transformation. To find the generator G of the full transformation, we apply Eq.(2.14) and integrate $\mathbf{u}$ with respect to $\mathbf{\Phi}$ with the help of a Fourier series. In sections 4 and 5 we show how to construct $\mathbf{u}(\mathbf{J}, \mathbf{\Phi})$ as a finite Fourier series,

$$\mathbf{u}(\mathbf{J}, \mathbf{\Phi}) = \sum_{\mathbf{m} \neq \mathbf{0}} \hat{\mathbf{u}}(\mathbf{m}, \mathbf{J}) e^{i\mathbf{m}\cdot\mathbf{\Phi}} \quad . \tag{2.20}$$

The corresponding series for G is

$$G(\mathbf{J}, \mathbf{\Phi}, 0) = \sum_{\mathbf{m} \neq \mathbf{0}} \hat{G}(\mathbf{m}, \mathbf{J}, 0) e^{i\mathbf{m}\cdot\mathbf{\Phi}} \quad . \tag{2.21}$$

In Eq.(2.21) we have arbitrarily omitted the $\mathbf{\Phi}-$independent term ($\mathbf{m} = \mathbf{0}$). This does not spoil generality, as we shall show presently. By Eq.(2.14) , the $j-$th component of $\mathbf{u}$ is

$$u_j(\mathbf{J}, \mathbf{\Phi}) = \sum i m_j \hat{G}(\mathbf{m}, \mathbf{J}, 0) e^{i\mathbf{m}\cdot\mathbf{\Phi}} \quad . \tag{2.22}$$

For any vector $\mathbf{m} \neq \mathbf{0}$ there is a j such that

$$\hat{G}(\mathbf{m}, \mathbf{J}, 0) = \hat{u}_j(\mathbf{m}, \mathbf{J})/im_j \ , \quad m_j \neq 0 \ . \tag{2.23}$$

The generating function defined by (2.23) and (2.21) allows us to complete the canonical transformation by defining

$$\mathcal{V}(\mathbf{J}, \mathbf{\Phi}) = (\mathbf{J}, \mathbf{\Psi}) \ , \tag{2.24}$$

where

$$\mathbf{\Psi} = \mathbf{\Phi} + G_{\mathbf{J}}(\mathbf{J}, \mathbf{\Phi}, 0) \ . \tag{2.25}$$

The complete transformation is

$$\mathcal{U} \circ \mathcal{V}^{-1}(\mathbf{J}, \mathbf{\Psi}) = (\mathbf{I}, \mathbf{\Phi}) \ . \tag{2.26}$$

If the transformation is ideal, so that $\mathbf{J}$ is constant, then the change in $\mathbf{\Psi}$ in one turn will give the tune $\boldsymbol{\nu}$:

$$\mathbf{\Psi}(2\pi) - \mathbf{\Psi}(0) = \mathbf{\Phi}(2\pi) - \mathbf{\Phi}(0) + G_{\mathbf{J}}(\mathbf{J}, \mathbf{\Phi}(2\pi), 0) - G_{\mathbf{J}}(\mathbf{J}, \mathbf{\Phi}(0), 0) = 2\pi\boldsymbol{\nu}(\mathbf{J}) \ . \tag{2.27}$$

If $\mathbf{J}$ is approximately constant, this equation will yield an approximation to the tune if we put $\mathbf{J}$ equal to its initial value $\mathbf{J}(0)$ and let $\mathbf{\Phi}(2\pi)$ be the angle value that evolves from $(\mathbf{J}(0), \mathbf{\Phi}(0))$ under the one-turn map. We use this method to obtain the tune numerically.

If G is modified by addition of a $\mathbf{\Phi}-$independent term,

$$\hat{G}(\mathbf{0}, \mathbf{J}, \theta) \quad , \tag{2.28}$$

the relation (2.27) is not changed, because such a term must be $2\pi-$periodic in θ. The local definition of $\mathbf{\Psi}$ would be changed, but not the increment of $\mathbf{\Psi}$ when θ advances by 2π.

The map $\mathcal{M}$ on original variables of course induces maps on the new variables through the transformations $\mathcal{U}$ and $\mathcal{V}$. We have

$$\mathcal{N}(\mathbf{J}, \mathbf{\Phi}) = \mathcal{U}^{-1} \circ \mathcal{M} \circ \mathcal{U}(\mathbf{J}, \mathbf{\Phi}) = (\mathbf{J}', \mathbf{\Phi}') \quad , \tag{2.29}$$

and

$$\mathcal{O}(\mathbf{J}, \mathbf{\Psi}) = \mathcal{V} \circ \mathcal{U}^{-1} \circ \mathcal{M} \circ \mathcal{U} \circ \mathcal{V}^{-1}(\mathbf{J}, \mathbf{\Psi}) = (\mathbf{J}', \mathbf{\Psi}') \quad . \tag{2.30}$$

These relations are obvious from the commutative diagram of Fig.1. For instance, Eq.(2.29) is obtained by noting that $\mathcal{N}$ followed by $\mathcal{U}$ produces the same result as $\mathcal{U}$ followed by $\mathcal{M}$; that is, $\mathcal{U} \circ \mathcal{N} = \mathcal{M} \circ \mathcal{U}$. Note also the nice symmetry of the diagram about its center line, associated with the fact that $\mathcal{U}$ and $\mathcal{V}$ are obtained from the two derivatives, $G_{\mathbf{\Phi}}$ and $G_{\mathbf{J}}$, of the same generating function.

Since we are mainly interested in the time evolution of $\mathbf{J}$, and less in the time evolution of $\mathbf{\Psi}$, we work mostly with the "half transformed" map $\mathcal{N}$, which is easier to evaluate than the "fully transformed" map $\mathcal{O}$. The evaluation of $\mathcal{N}$ requires the computation of $\mathcal{U}^{-1}(\mathbf{J}', \mathbf{\Phi}')$, which is not available from an explicit formula. In Section 5 we point out that this quantity is easily computed by Newton's method.

3. LONG-TERM BOUNDS

The map $\mathcal{N}$ of (2.29) gives the change in $\mathbf{J}$ over N_o turns. We apply an essentially trivial argument to find bounds on the change in $\mathbf{J}$ over a number of turns N much greater than N_o. We find the largest change in $\mathbf{J}$ that can occur over N_o turns, and then imagine the worst possible case in which the change over pN_o turns is just p times the largest change over N_o turns. We are able to succeed with this coarse argument only by constructing such a good canonical transformation that the change of $\mathbf{J}$ in N_o turns is extremely small.

It should be recognized that the resulting bounds are for the N_o-turn map, and make no direct reference to what may happen between turn kN_o and turn $(k+1)N_o$. It is conceivable that the orbit could leave the desired region during this interim, but nevertheless return to it by turn $(k+1)N_o$.[30] In practice we rule out any harm from such an effect, since the N_o-turn map is evaluated by integration of the equations of motion in small steps. The numerical integrator is arranged to give a signal if the orbit leaves a prescribed region.

We define a domain Ω of phase space, and a smaller domain $\Omega_o \subset \Omega$ as follows:

$$\Omega = \left\{\mathbf{J}, \mathbf{\Phi} \;\middle|\; |J_i - \hat{J}_i| < \Delta J_i,\;\; 0 \le \Phi_i \le 2\pi,\;\; i = 1, 2, \cdots, d\right\} \;, \tag{3.1}$$

$$\Omega_o = \left\{\mathbf{J}, \mathbf{\Phi} \;\middle|\; |J_i - \hat{J}_i| < \lambda_i \Delta J_i,\;\; 0 \le \Phi_i \le 2\pi,\;\; i = 1, 2, \cdots, d\right\} \;,$$

$$0 < \lambda_i < 1 \;. \tag{3.2}$$

The fixed vector $\hat{\mathbf{J}} = \{\hat{J}_i\}$ defines an "average amplitude of interest" for our stability studies. Now suppose that for all $(\mathbf{J}, \mathbf{\Phi}) \in \Omega$ the N_o–turn map (2.29) is such that

$$|J_i - J_i'| < \delta J_i, \quad i = 1, 2, \cdots, d \quad . \tag{3.3}$$

Any orbit with initial condition $(\mathbf{J}(0), \mathbf{\Phi}(0))$ in Ω_o will stay within the larger region Ω for at least N turns, where

$$N = pN_o \quad , \tag{3.4}$$

and p is the largest integer such that

$$p\delta J_i < (1 - \lambda_i)\Delta J_i \quad , \quad i = 1, 2, \cdots, d \quad . \tag{3.5}$$

That is, a trajectory cannot cross the annulus between Ω and Ω_o in fewer than $(p+1)N_o$ turns, where

$$p + 1 \geq A(\Omega, \Omega_o) = \min_i \frac{(1 - \lambda_i)\Delta J_i}{\delta J_i} \quad . \tag{3.6}$$

We may think of the quantity $A(\Omega, \Omega_o)$ of (3.6) as an "amplification factor" that gives a bound for N turns in terms of a bound for a smaller number of turns N_o. In the example of Section 6 we find an A of around 10^4, and the value is substantially independent of N_o for N_o up to at least 10^4. The discovery of such large amplification factors is the basis for our interest in the method.

The best choice of the regions Ω and Ω_o is a matter that depends both on the particular system studied and on the goal of the study. In general one can expect that $A(\Omega, \Omega_o)$ will initially be an increasing function of ΔJ_i, until Ω gets so large

that some source of instabilty is encountered (for instance, a broad resonance), causing an increase in δJ_i and eventual decrease of A. On the other hand, Ω might become too large to be suitable for the conditions of the problem. In an accelerator problem it might reach into a region of phase space beyond the physical aperture of the machine, and would then be of no interest.

Simple regions like (3.1), (3.2) are not necessarily the most relevant for practical stability studies. In the different stages of operation of an accelerator the particles visit various regions of phase space. Generally, one would like to ensure stability for any action value from $\mathbf{J} = 0$ out to some limit. In two degrees of freedom, this limit would be described by some curve in the $J_1 - J_2$ plane, of course just in the first quadrant of that plane since the J_i are non-negative by definition. For example, let us take the curve to be made of two straight line segments, parallel to the J_1 and J_2 axes. Further, let us consider two such curves and the L-shaped region $\mathcal{L}$ between them, as shown in Figure 2. Suppose that we could show, by arguments as above, that any trajectory starting near the inner edge of $\mathcal{L}$ (in the darkened band $\mathcal{B}$ of the figure) cannot cross to the outer edge of $\mathcal{L}$ in pN_o turns. Suppose also that any trajectory starting in $\mathcal{L}_o$, the region enclosed by $\mathcal{L}$, cannot move more than the width of $\mathcal{B}$ in N_o turns. If $N = pN_o$ is large it then follows that $\mathcal{L}$ forms an effective barrier to motion out of $\mathcal{L}_o$.

This is reminiscent of the absolute confinement of trajectories by K.A.M. surfaces that occurs in low-dimensional systems ($d \leq 2$ for autonomous systems, $d = 1$ for time dependent Hamiltonians of the form (2.1)). Although in higher dimensions we do not have absolute confinement, we may have confinement for a very long time by a barrier region such as $\mathcal{L}$, which can be viewed as a "thickened surface."

We now state this argument more precisely for a phase space of arbitrary dimension, and comment on its practical realization. Referring to Figure 2, we define

$$\mathcal{L} = \left\{ \mathbf{J}, \mathbf{\Phi} \mid J_i^{(0)} < J_i < J_i^{(1)}, \;\; 0 \leq \Phi_i \leq 2\pi \right\} \;\; , \tag{3.7}$$

$$\mathcal{B} = \left\{ \mathbf{J}, \mathbf{\Phi} \mid J_i^{(0)} < J_i < J_i^{(0)} + \eta_i, \;\; 0 \leq \Phi_i \leq 2\pi \right\} \;\; , \tag{3.8}$$

$$\mathcal{L}_o = \left\{ \mathbf{J}, \mathbf{\Phi} \mid J_i \leq J_i^{(0)}, \;\; 0 \leq \Phi_i \leq 2\pi \right\} \;\; , \tag{3.9}$$

$$0 < \eta_i < J_i^{(1)} - J_i^{(0)} \;\; . \tag{3.10}$$

Here and in the following it is understood that i runs from 1 to d, for d degrees of freedom. Assume that the N_o–turn map (2.29) gives

$$J_i' - J_i < \eta_i \;\; , \quad (\mathbf{J}, \mathbf{\Phi}) \in \mathcal{L}_o \;\; , \tag{3.11}$$

and that for some $\delta J_i > 0$,

$$J_i' - J_i < \delta J_i \;\; , \quad (\mathbf{J}, \mathbf{\Phi}) \in \mathcal{L}. \tag{3.12}$$

Then any trajectory with initial condition $(\mathbf{J}(0), \mathbf{\Phi}(0)) \in \mathcal{L}_o$ will satisfy

$$J_i < J_i^{(1)} \tag{3.13}$$

for $N = pN_o$ turns, where p is the largest integer such that

$$p\delta J_i < J_i^{(1)} - J_i^{(0)} - \eta_i \;\; , \tag{3.14}$$

hence

$$p+1 \geq \min_i \frac{J_i^{(1)} - J_i^{(0)} - \eta_i}{\delta J_i} \quad . \tag{3.15}$$

Notice that we have not put absolute value signs on the increments $J_i' - J_i$, since there is no objection to large negative increments.

In a numerical application of this argument it is advantageous to take η_i considerably larger than δJ_i. Verification of the inequality (3.11) can then be done at much smaller expense than is required for verification of $\Leftarrow \exists \not\swarrow \infty \in \Rightarrow$. In region $\mathcal{L}_o$ one can take fewer mesh points in $\mathbf{J}$, or fewer Fourier modes in (2.20) . The width η_i of the band $\mathcal{B}$ can still be much less than $J_i^{(1)} - J_i^{(0)}$, so that the value of η_i has little impact on the bound (3.15) .

In any practical case it is necessary to have statements about the original laboratory variable $\mathbf{I}$, rather than $\mathbf{J}$. The methods of Section 5 provide a way of going back and forth between $\mathbf{J}$ and $\mathbf{I}$. For any $(\mathbf{I}, \mathbf{\Phi})$ one can find the corresponding $\mathbf{J}$ through numerical evaluation of $\mathcal{U}^{-1}$, and vice versa.

4. COMPUTATION OF APPROXIMATE INVARIANT TORI

In this section we describe a method[24,16] for computing close approximations to invariant tori, beginning with the map $\mathcal{M}(\mathbf{I}, \mathbf{\Phi}) = (\mathbf{I}', \mathbf{\Phi}')$ for $N_o = 1$. To simplify notation and give numerical examples we take two degrees of freedom, $d = 2$. A good feature of the method is that it generalizes obviously to any d.

Starting with initial condition $(\mathbf{I}(0), \mathbf{\Phi}(0))$, we follow a single orbit by iterating the map P times, recording the coordinates at each iterate,

$$(\mathbf{I}, \mathbf{\Phi})_j \quad , \quad j = 1, 2, \cdots, P \quad . \tag{4.1}$$

Suppose that the orbit is not in a region of wide-spread chaos, as is usually true in accelerator physics. If the orbit is not on a resonance, or is on a resonance of very high order, the angular coordinates $\mathbf{\Phi}_j$ will be distributed rather densely in the (Φ_1, Φ_2) plane at large P. In Figure 3 we plot 4000 values of $\mathbf{\Phi}$ on a trajectory of the system treated in Section 6. In Figure 4 we show the contrasting behavior of $\mathbf{\Phi}$ on a resonant trajectory. In Figure 5 we plot the points $(I_1, \mathbf{\Phi}_1, \mathbf{\Phi}_2)$ in three dimensions for a nonresonant trajectory (not distinguishable from a resonant orbit of very high order). Figure 6 shows the corresponding points $(I_2, \mathbf{\Phi}_1, \mathbf{\Phi}_2)$. Excluding obvious resonant cases, we attempt to fit the points $(\mathbf{I}, \mathbf{\Phi})_j$ to a surface represented as a finite Fourier series,

$$\mathbf{I} = \sum_{\mathbf{m} \in S} \hat{\mathbf{u}}(\mathbf{m}) e^{i\mathbf{m}\cdot\mathbf{\Phi}} \quad . \tag{4.2}$$

The $\mathbf{\Phi}-$independent term $(\mathbf{m} = 0)$ will be identified with the approximate invariant action $\mathbf{J}$, in accord with (2.12) and (2.20).

In our examples of interest the set S of Fourier modes in (4.2) usually includes modes up to $m = 20$ or so in each variable, but for some purposes our maximum m may be as low as 10 or as high as 30. Thus, we have a fairly large set of coefficients to determine, and that is a problem in itself. Moreover, the values of $\mathbf{\Phi}$ are scattered unpredictably. For that reason we cannot use an elementary discrete Fourier Transform (say an FFT), which requires values of $\mathbf{\Phi}$ on a uniform rectangular mesh to compute the coefficients $\hat{\mathbf{u}}(\mathbf{m})$.

To handle the problem of scattered abscissae, we replace the unknowns $\hat{\mathbf{u}}(\mathbf{m})$ with a new set of unknowns, namely the values of the function $\mathbf{I}(\mathbf{\Phi})$ on a uniform mesh on $\mathbf{\Phi}$ space. The matrix that relates these quantities to the data points $\mathbf{I}(\mathbf{\Phi}_j)$

is close to the unit matrix (provided that we use only a certain subset of the data points), and that implies that one can solve for the unknowns by iteration. The iterative method avoids solution of the large linear system by a direct method (say Gaussian elimination) which would be too expensive.

As a one-dimensional model of our problem consider

$$I(\phi_j) = \sum_{m=-M}^{m=M} \hat{u}(m) e^{im\phi_j} \quad , \quad j = 0, 1, \cdots, K-1 \tag{4.3}$$

for some set of scattered points $\{\phi_j\}$. We replace $\hat{u}(m)$ with the discrete Fourier transform of I:

$$\hat{u}(m) = \frac{1}{K} \sum_{k=0}^{K-1} \exp(\frac{2\pi imk}{K}) I(\frac{2\pi k}{K}) \approx \frac{1}{2\pi} \int_0^{2\pi} e^{im\phi} I(\phi) d\phi \quad . \tag{4.4}$$

Now substitute (4.4) in (4.3) , reverse the order of the m and k sums, and choose M so that $K = 2M + 1$. Evaluating the sum over m as a geometric series we find

$$I(\phi_j) = \sum_{k=0}^{K-1} \frac{\sin[\pi(x(j) - k)]}{K \sin[\pi(x(j) - k)/K]} \, I(\frac{2\pi k}{K}) \quad , \tag{4.5}$$

where $x(j)$ is a normalized coordinate replacing ϕ_j,

$$\phi_j = 2\pi x(j)/K \quad . \tag{4.6}$$

The matrix $D = \{D_{jk}\}$ with

$$D_{jk} = \frac{\sin[\pi(x(j) - k)]}{K \sin[\pi(x(j) - k)/K]} \tag{4.7}$$

is a discrete analog of the Lejeune-Dirichlet kernel that is used in Fourier analysis to express partial sums of Fourier series.

The interesting aspect of D is that it is close to the unit matrix if the ϕ_j are close to the evenly spaced mesh points $2\pi j/K$ of the discrete Fourier transform; equivalently,

$$x(j) \approx j \quad \Rightarrow \quad D_{jk} \approx \delta_{jk} \ . \tag{4.8}$$

We can ensure that (4.8) holds for all (j,k) if we compute a sufficiently long orbit and admit to the fitting procedure just those points with angles ϕ_j sufficiently close to the evenly spaced mesh points. In matrix notation the $K \times K$ system (4.5) takes the form

$$I = (1 - D)I + \hat{I} \ , \tag{4.9}$$

where

$$I = \{I(2\pi j/K)\} \ , \quad \hat{I} = \{I(\phi_j)\} \ . \tag{4.10}$$

Provided that $1 - D$ has sufficiently small norm, (4.10) can be solved by simple iteration, beginning with $\hat{I}$ as a first guess. We actually apply a modified Gauss-Seidel method[31], which is more effective than simple iteration. With the p-th iterate denoted by $I^{(p)}$ our iteration is

$$I_j^{(p+1)} = \sum_{k=0}^{j-1} (\delta_{jk} - D_{jk}) I_k^{(p+1)} + \sum_{k=j}^{K-1} (\delta_{jk} - D_{jk}) I_k^{(p)} + \hat{I}_j \ . \tag{4.11}$$

This scheme results from (4.9) and the observation that for evaluation of the j-th component of $I^{(p+1)}$, the updated values of prior components are already available, namely $I_k^{(p+1)}$ for $k = 0, 1, \cdots, j-1$. In the ordinary Gauss-Seidel method, D and $\hat{I}$ in (4.9) are multiplied by Δ^{-1}, where Δ is the diagonal part of D. For some reason, our iteration is slightly better in the present case.

In two degrees of freedom we have two surfaces to fit, corresponding to the two components of $\mathbf{I} = (I_1, I_2)$. We try to solve for

$$\mathbf{I}(2\pi k_1/K_1,\ 2\pi k_2/K_2) \quad . \tag{4.12}$$

From the sequence (4.1) we select a subsequence of $K_1 K_2$ points having angular coordinates in one to one correspondence with the evenly spaced mesh points,

$$(2\pi j_1/K_1,\ 2\pi j_2/K_2) \quad , \quad j_i = 0, 1, \cdots, K_i - 1 \quad . \tag{4.13}$$

The correspondence is set up by choosing one and only one point close to each mesh point in the sense

$$|x_i - j_i| < r_i \quad , \quad 0 < r_i \leq 1/2 \quad , \quad i = 1, 2 \quad , \tag{4.14}$$

where the x_i are normalized values of the angular coordinates from (4.1) :

$$\Phi_i = 2\pi x_i / K_i \quad . \tag{4.15}$$

The normalized coordinates satisfying (4.14) will be denoted as $x_i(j_1, j_2)$, and the corresponding original coordinates by $\Phi_i(j_1, j_2)$.

To apply the iteration (4.11) we introduce a map of the index pair (j_1, j_2) into a single index j, and define the unknowns,

$$\mathbf{I}_j = \mathbf{I}(2\pi j_1/K_1,\ 2\pi j_2/K_2) \quad , \tag{4.16}$$

and the data,

$$\hat{\mathbf{I}}_j = \mathbf{I}(\Phi_1(j_1, j_2), \Phi_2(j_1, j_2)) \quad . \tag{4.17}$$

The bold face characters are a reminder that there are two surfaces to be determined. The matrix D analogous to (4.4) is the same for both surfaces, and has the form

$$D_{jk} = \frac{\sin[\pi(x_1(j_1,j_2) - k_1)]}{K_1 \sin[\pi(x_1(j_1,j_2) - k_1)/K_1]} \quad \frac{\sin[\pi(x_2(j_1,j_2) - k_2)]}{K_2 \sin[\pi(x_2(j_1,j_2) - k_2)/K_2]} \quad . \tag{4.18}$$

In practice it may be difficult to store this large matrix in the computer. We resorted to storing only the two factors of (4.18) , each as a three-dimensional array.

The "radii" r_i of the neighborhoods of mesh points, as defined in (4.14) , determine the rate of convergence of the iteration (4.11) , smaller values giving faster convergence. In all of our examples we have found convergence with $r_1 = r_2 = 1/2$, which means that the neighborhood (4.14) is the same size as a cell of the mesh. In the examples of Section 6 there was an advantage in using smaller values of r_i to increase the rate of convergence; our typical choice was $r_1 = r_2 = 0.3$. This advantage disappears in cases where iteration of the map $\mathcal{M}$ is more expensive, since the length of the sequence (4.1) to produce the required points increases sharply as r_i is decreased.

An interesting property of this method is that it provides a convenient way to filter out resonances. A low-order resonant orbit such as that of Figure 4 will not come close to every mesh point and hence will never satisfy (4.14). A resonance of higher order may satisfy (4.14) , but it has less and less chance of doing so as r_i is decreased. In our examples, any resonant orbit that satisfies (4.14) with $r_1 = r_2 = 0.3$ and $M_1 = M_2 = 20$ is of such high order that its resonant character has no significance in our discussion; for our purposes it is indistinguishable from an orbit lying on an invariant torus.

After Eq. (4.9) is solved, we find the the Fourier amplitudes $\hat{\mathbf{u}}(\mathbf{m})$ of (4.2) by the discrete Fourier transform (4.4). It is easy to see that the resulting surface (4.2) actually passes through the data points (provided that (4.9) is solved exactly).

5. INTERPOLATION AND INVERSION OF NONLINEAR FUNCTIONS

The basic object needed to find long-term bounds is the change of variable $\mathcal{U}(\mathbf{J}, \mathbf{\Phi}) = (\mathbf{I}, \mathbf{\Phi})$. The method of the previous section gives $\mathcal{U}$ in the form

$$\mathbf{I} = \sum_{\mathbf{m} \in \mathcal{S}} \hat{\mathbf{u}}(\mathbf{m}, \mathbf{J}) e^{i\mathbf{m}\cdot\mathbf{\Phi}} \quad . \tag{5.1}$$

By definition, the parameter $\mathbf{J}$ for this surface is

$$\mathbf{J} = \hat{\mathbf{u}}(\mathbf{0}) \quad , \tag{5.2}$$

a quantity which is not known until all the Fourier coefficients have been determined by fitting data. We observe in computations, and require in principle, that there is a one-to-one correspondence between initial values $\mathbf{I}(\theta = 0)$ of fitted orbits and values of $\mathbf{J}$, the correspondence being made at a fixed value of the initial angle $\mathbf{\Phi}(\theta = 0)$. The choice of the fixed angle is immaterial; we take it to be zero for all fitted orbits, and adopt the notation $\mathbf{I}_o$ for the corresponding initial action:

$$(\mathbf{I}_o, \mathbf{0}) = (\mathbf{I}(\theta), \mathbf{\Phi}(\theta))_{\theta=0} \quad . \tag{5.3}$$

If we fit n orbits, all with different values $\mathbf{I}_{oi}$ of $\mathbf{I}_o$, we obtain

$$\mathbf{I} = \mathbf{J}_i + \sum_{\mathbf{m}\neq\mathbf{0}} \hat{\mathbf{u}}(\mathbf{m},\mathbf{J}_i)e^{i\mathbf{m}\cdot\mathbf{\Phi}} \quad , \quad i = 1,2,\cdots,n \quad , \tag{5.4}$$

the n values $\mathbf{J}_i$ being all distinct.

In order to define the transformation (5.1) as a smooth function of $\mathbf{J}$ in a region of phase space, we seek a smooth interpolation of the Fourier coefficients $\hat{\mathbf{u}}(\mathbf{m},\mathbf{J}_i)$. The $\mathbf{J}_i$ are not exactly predictable, but we expect and find empirically that there is a nearly linear dependence of $\mathbf{J}$ on $\mathbf{I}_o$ in domains of interest (except near a broad resonance where there can be jogs in the linear behavior). This means that one can control fairly well the distribution of the $\mathbf{J}_i$ by appropriate choice of the $\mathbf{I}_{oi}$ and thereby make a reasonable choice of points to interpolate. We usually put the $\mathbf{J}_i$ near the points of a regular Cartesian grid, but since we can not put them precisely at such points interpolation in one dimension at a time is not possible. We are therefore led to a method like that used in the preceeding section to fit data at scattered angles. The desired function of $\mathbf{J}$ is expanded as a linear combination of basis functions, and linear equations are solved to determine the coefficients.

The basis functions themselves will be tensor products of functions of one variable. For the latter we choose basis functions for cubic splines[32] on the interval $[0,1]$, with $s+1$ evenly spaced knots,

$$x_i = i/s \quad , \quad i = 0,1,\cdots,s \quad . \tag{5.5}$$

We define a spline function $f(x)$ to be a piecewise polynomial function that is cubic in each interval $[x_i, x_{i+1}]$, has a continuous second derivative at $x_1, x_3, \cdots, x_{s-1}$,

and a continuous third derivative at x_1 and x_{s-1}. We define $\beta_i(x)$ to be that spline function which is equal to 1 at x_i and 0 at the other knots,

$$\beta_i(x_j) = \delta_{ij} \quad , \quad i,j = 0,1,\cdots,s \quad . \tag{5.6}$$

A spline function is uniquely defined by its values at the knots, as can be seen by counting the continuity conditions. It follows that $f(x)$ may be represented as

$$f(x) = \sum_{i=0}^{s} f(x_i)\beta_i(x) \quad , \tag{5.7}$$

since the right hand side is a spline function, and has the correct values at the knots. The coefficients of the cubic polynomials that make up the basis splines β_i can be obtained by applying standard codes (for instance CUBSPL from Ref. 32) and the defining property (5.6).

Now suppose that $f(x)$ is not a spline function, and that its values are known at $s+1$ distinct points ξ_i, different from the x_i and in general not equally spaced. We can try to approximate $f(x)$ as

$$f(x) \approx \hat{f}(x) = \sum_{i=0}^{s} \lambda_i \beta_i(x) \quad , \tag{5.8}$$

defining the λ_i as solutions of the linear equations

$$f(\xi_j) = \sum_{i=0}^{s} \lambda_i \beta_i(\xi_j) \quad , \quad j = 0,1,\cdots,s \quad . \tag{5.9}$$

Then $\hat{f}(x)$ interpolates the given values, $\hat{f}(\xi_i) = f(\xi_i)$, and $\lambda_i = \hat{f}(x_i)$.

If we were working in one dimension, it would clearly be more convenient to take the spline knots at the ξ_i, so as to obtain $\lambda_i = f(\xi_i)$ without solving equations. With scattered abscissae in two or more dimensions there is no such possibility, but the above method can still be applied. In two dimensions we apply spline approximation first in one variable and then in the other to obtain

$$f(x_1, x_2) \approx \hat{f}(x_1, x_2) = \sum_{i=0}^{s_1} \sum_{j=0}^{s_2} \lambda_{ij} \beta_i^{(1)}(x_1) \beta_j^{(2)}(x_2) \quad , \tag{5.10}$$

For scattered data at points (ξ_k, η_k) the equations to fix the coefficients are

$$f(\xi_k, \eta_k) = \sum_{i=0}^{s_1} \sum_{j=0}^{s_2} \lambda_{ij} \beta_i^{(1)}(\xi_k) \beta_j^{(2)}(\eta_k) \quad . \tag{5.11}$$

As before, $\hat{f}$ interpolates the given values $f(\xi_k, \eta_k)$, and $\lambda_{ij} = \hat{f}(\xi_k, \eta_k)$.

In the following we use the scheme based on (5.10) , (5.11) for approximating several different functions. In each case a rectangular domain for the vector variable of interest is mapped onto $[0,1] \times [0,1]$, so that the same basis functions can be used for all interpolations. For interpolation in each component of $\mathbf{J}$ the map to take $J \in [J_a, J_b]$ into $x \in [0,1]$ is

$$x = \frac{J^{1/2} - J_a^{1/2}}{J_b^{1/2} - J_a^{1/2}} \quad . \tag{5.12}$$

The use of $J^{1/2}$ rather than J in (5.12) is to take account of the fact, familiar from perturbation theory, that invariant surfaces contain powers of $J^{1/2}$ at small J. At the larger values of J considered in Section 6, a linear map is probably just as suitable as (5.12).

Interpolation of scattered data can be used to invert nonlinear functions numerically. Given the values of a $1:1$ function $f: x \to f(x)$ on a finite set of points, which is to say a set of pairs (x_i, f_i), one can interpolate in either direction: find a smooth function $\hat{f}(x)$ with $\hat{f}(x_i) = f_i$, or a smooth function $\hat{x}(f)$ with $\hat{x}(f_i) = x_i$. In Section 6 we use this method to find $\mathbf{J}(\boldsymbol{\nu})$, the action as a function of the tune $\boldsymbol{\nu}$. The function $\boldsymbol{\nu}(\mathbf{J})$ is first evaluated on a mesh in $\mathbf{J}$ space by application of (2.27).

Having determined $\mathcal{U}(\mathbf{J}, \boldsymbol{\Phi})$ as a finite Fourier series in $\boldsymbol{\Phi}$ with coefficients as spline functions in $\mathbf{J}$, we can now turn attention to evaluation of the map $\mathcal{N}$ as defined in (2.29). Referring to (2.29) , (2.30) , and Figure 1, we see that evaluation of $\mathcal{N}(\mathbf{J}, \boldsymbol{\Phi})$ requires evaluation of $\mathcal{U}^{-1}(\mathbf{I}', \boldsymbol{\Phi}')$, which is to say solution of the following equation for $\mathbf{J}'$:

$$\mathbf{I}' = \mathbf{J}' + \mathbf{u}(\mathbf{J}', \boldsymbol{\Phi}') \quad . \tag{5.13}$$

This equation is easily solved by Newton's method. Since $\mathbf{J}'$ is typically very close to $\mathbf{J}$, a Newton iteration beginning with $\mathbf{J}$ as zeroth iterate converges quickly. In fact, the first iterate is an adequate solution for much of the work in Section 6; it is given by

$$\mathbf{J}' \approx \mathbf{J} + [1 + \mathbf{u}_{\mathbf{J}}(\mathbf{J}, \boldsymbol{\Phi}')]^{-1}[\mathbf{I}' - \mathbf{J} - \mathbf{u}(\mathbf{J}, \boldsymbol{\Phi}')] \quad . \tag{5.14}$$

Here $\mathbf{u}_{\mathbf{J}}$ may be computed analytically by differentiating the spline functions that express the $\mathbf{J}$ dependence of $\mathbf{u}$. Thus, we have all the ingredients to evaluate $\mathcal{N}$ through formula (2.29).

6. LONG-TERM BOUNDS FOR A REGION IN WHICH ALL RESONANCES ARE WEAK

We illustrate our method on a problem of basic interest in accelerator theory, the so-called betatron motion in a cyclic accelerator or storage ring. It consists of oscillations in two degrees of freedom transverse to the direction of the beam. The coordinates $x_i, i = 1, 2$ are transverse displacements from a closed reference orbit of circumference $2\pi R$. The corresponding canonical momenta are $p_i = dx_i/ds$, where $s = R\theta$ measures arc length along the reference orbit and serves both as the independent variable of Hamilton's equations and as a coordinate to specify the longitudinal location of the particle. The motion is essentially equivalent to perturbed harmonic motion, with the nonlinear perturbation arising from sextupole magnets that are introduced to compensate the dependence of the focusing system on the longitudinal momentum. The field of a sextupole is concentrated in a small region of s, and gives a term in the perturbation V proportional to $x_1^3 - 3x_1x_2^2$. Thus, the contribution of a single sextupole to the evolution in s resembles a four-dimensional quadratic map. Owing to the s-dependence of the sextupole fields, the Hamiltonian depends periodically on s, and the system effectively has a 5-dimensional phase space ($2\frac{1}{2}$ degrees of freedom).

We choose a relatively simple accelerator model, containing only four sextupoles, which allows us to make rather extensive numerical experiments at low cost. The example corresponds to one cell of the lattice (configuration of magnets) of a forthcoming electron storage ring, the Berkeley Advanced Light Source (ALS). Our model is not intended as a good approximation to the actual machine, since the full lattice has 12 cells and additional complications that we do not account for; also, we neglect synchrotron oscillations, which have an important effect on

long-term behavior. Nevertheless, the example is of real practical interest in that it involves realistic parameters leading to strong excitation of nonlinear resonances of various orders, a matter of concern in most accelerators. In particular, it includes resonance phenomena similar to those induced by high-order magnetic multipoles associated with superconducting magnets in large hadron colliders. Thinking of our example as being relevant to hadron machines, we try to predict stability for 10^8 turns. Large-amplitude stability is required for far fewer turns in electron machines (say 10^4), owing to damping of oscillations by synchrotron radiation.

For a fully realistic treatment of accelerators it will be necessary to include an additional degree of freedom for synchrotron motion, which is to say oscillations in energy with frequency much less than the betatron frequencies. There is reason to believe that this can be done after further work, but for the present it is more important to evaluate and understand the method in the simplest non-trivial context. In formal aspects the method is the same in any dimension.

The Hamiltonian and accelerator parameters for our model are given in Appendix A. For the present discussion the reader only has to know that this Hamiltonian defines the time evolution map $\mathcal{M}$ of Eq. (2.11) via numerical integration of Hamiltonian's equations. The integration is done by the fourth order explicit symplectic algorithm of Ref. 27, with one symplectic integration step per sextupole magnet. Increasing the accuracy by using two steps per magnet has no appreciable effect.

The first step of the computation is to determine a set of approximately invariant tori by the method of Section 4. We work in a rectangular region Ω of $\mathbf{J}$ space as follows:

$$2.51 \cdot 10^{-6} m \leq J_1 \leq 2.82 \cdot 10^{-6} m$$
$$1.34 \cdot 10^{-6} m \leq J_2 \leq 1.64 \cdot 10^{-6} m \tag{6.1}$$

The action $\mathbf{J}$ is defined so as to have the dimension of length, and is measured in meters. It is the usual action divided by the longitudinal beam momentum. The region Ω is a domain of rather strong nonlinearity. This is clear from Figures 5 and 6, which show sets of points $(\mathbf{I}, \mathbf{\Phi})$ for a $\mathbf{J}$ in this region. We compute tori at 25 points in the region (6.1). The points are those marked with an asterisk in Figure 7. They lie close to the points of a 5×5 Cartesian grid.

The points do not follow a Cartesian grid exactly, and we cannot make them do so, since the $\mathbf{J}$ of a chosen grid point may correspond to a resonance of sufficient width to preclude construction of a "good" torus. A good torus is defined loosely as one that is invariant under the map $\mathcal{M}$ to a standard of accuracy chosen for the problem at hand. For instance, the 25 good tori for the points marked in Figure 7 are all invariant to 2 parts in 10^6 or better. We decided on this standard of accuracy by experimenting with the number of Fourier modes in the torus representation (4.2). The standard adopted is roughly the best that could be achieved at reasonable cost. It is obtained by including all Fourier modes up to the 20th,

$$|m_1|, \quad |m_2| \quad \leq \quad M = 20 \quad . \tag{6.2}$$

Increasing the maximum mode number M to 30 gives little improvement at high cost, whereas decreasing it to 10 degrades the accuracy by a factor of 10 or more. (Actually, a computation with $M = 10$ already gives bounds of significant magnitude, and is a great deal cheaper).

As was explained in Section 5, the initial actions $\mathbf{I}_o$ defined in (5.3) are the primary inputs to the program that finds tori, not the desired values of $\mathbf{J}$. Moreover,

the program may fail at a particular $\mathbf{I}_o$, owing to the presence of a resonance. Since resonances are found fairly often, the computer program is arranged so that after a failure it automatically shifts the value of $\mathbf{I}_o$ by a small amount and tries again. Failure is declared when a full set of orbit points close to the Φ mesh points is not obtained in a specified number of turns N_t; i.e., when there are not enough points x_i to satisfy (4.14) for all j_i. We typically choose $N_t = 10000$ for $r_i = 0.5$. In region (6.1) the required shifts $\Delta\mathbf{I}_o$ to overcome failure are quite small, as can be seen from Figure 5. We tried to put the points on a regular Cartesian grid, and succeeded quite well except for the point near the intersection of six resonance lines at the right of the figure.

To find the required values of $\mathbf{I}_o$ to produce desired $\mathbf{J}$ values, up to small shifts, we exploit the approximately linear relation between $\mathbf{I}_o$ and $\mathbf{J}$. We run the torus fitting program for a few values of $\mathbf{I}_o$ near the region of interest, and use the resulting values of $\mathbf{J}$ to make a least-squares fit to the coefficients in a linear formula giving $\mathbf{I}_o$ as a function of $\mathbf{J}$. This calculation can be done at low cost, since only a few Fourier modes are needed to determine $\mathbf{J}$ with adequate accuracy.

Having determined tori on a (slightly irregular) mesh in $\mathbf{J}$ space, we follow the interpolation methods of Section 5 to define the canonical transformation for all $\mathbf{J}$ in the region Ω. We can then find the tune $\boldsymbol{\nu}(\mathbf{J})$ by the method of Eq. (2.27), and the inverse function $\mathbf{J}(\boldsymbol{\nu})$ by the interpolation technique described near the end of Section 5. The function $\boldsymbol{\nu}(\mathbf{J})$ is locally nearly linear, so that the boundary of the rectangle Ω is mapped by $\boldsymbol{\nu}(\mathbf{J})$ into a figure Ξ that is nearly a parallelogram, as shown in Figure 8. Our program automatically finds all resonant tune lines,

up to a certain order, that pass through Ξ. The resonant tune lines are given by the equations

$$\begin{aligned} m_1\nu_1 + m_2\nu_2 &= p \ , \\ |m_1|,\ |m_2| &\leq \tilde{M} \ , \end{aligned} \tag{6.3}$$

where m_i and p are integers. These resonance lines are mapped into the $\mathbf{J}$ plane by applying the spline representation of $\mathbf{J}(\boldsymbol{\nu})$. Figure 7 shows the resulting lines in the $\mathbf{J}$-plane; all resonances in Ω with $|m_i| \leq 20$ are plotted, along with their mode numbers $[m_1, m_2]$. Figure 9 shows a similar plot, computed less accurately, for a larger region of the $\mathbf{J}$-plane. Here some curvature of the resonance lines is visible. Figure 10 is for the same large region, but with mode numbers restricted to $|m_i| \leq 10$.

The computed lines in the $\mathbf{J}$-plane serve to locate the resonances accurately, even in the case of very narrow resonances of high order. To test accuracy of a line, we track an orbit with initial condition on that line, and plot the values of the original angle variables (Φ_1, Φ_2) at each turn. In Figure 11 we show the result for the [17, 16] resonance of Figure 7. The points apparently lie on curves, having 17 intersections with the Φ_1 axis and 16 with the Φ_2 axis, as predicted. The corresponding curves for the new angles, (Ψ_1, Ψ_2), would be nearly straight lines.

We can now proceed to the main problem in finding long-term bounds, which is to estimate the change in $\mathbf{J}$ on an orbit of N_0 turns, for any initial condition in Ω. We must investigate $\mathbf{J}' - \mathbf{J}$, where $(\mathbf{J}', \boldsymbol{\Phi}') = \mathcal{N}(\mathbf{J}, \boldsymbol{\Phi})$, for all $\mathbf{J} \in \Omega$ and all $\boldsymbol{\Phi}$. The map $\mathcal{N}$ is obtained from the time evolution map $\mathcal{M}$ of the original variables, by using the change of variable $\mathcal{U}$ and its inverse, in accord with Figure 1 and Eq. (2.29). To evaluate $\mathcal{U}^{-1}$ we use the lowest order Newton method (5.14), after verifying that higher order Newton iterates would produce no change in our

conclusions. (If we had to deal with a high power of $\mathcal{N}$, more accuracy might be needed, but all we need is a rough value for the first power).

To evaluate $\mathcal{U}$ and $\mathcal{U}^{-1}$ we must sum the Fourier series for $\mathbf{u}$ and $\mathbf{u_J}$. To minimize the cost of summations we of course use the reality property $\hat{\mathbf{u}}(\mathbf{m},\mathbf{J}) = \hat{\mathbf{u}}(-\mathbf{m},\mathbf{J})^*$ to eliminate almost half of the terms in the series. Furthermore, we exploit the fact that many of the Fourier amplitudes are negligible. We throw away all amplitudes that are smaller in magnitude than a fraction ϵ of the largest amplitude $\hat{\mathbf{u}}(\mathbf{m},\mathbf{J}_i)$, $\mathbf{m} \neq 0$, with a typical choice for ϵ being 10^{-7}. This eliminates at least two thirds of the modes, without affecting the quality of the canonical transformation. This step is not equivalent to using a lower maximum mode number; some high modes are important.

A further reduction, which saves storage if not computation time, is achieved by noting that the two components of $\mathbf{u}$ should both come from derivatives of the same generating function G, according to (2.14). Thus,

$$\hat{u}_2\,(m_1,m_2,\mathbf{J}) = \frac{m_2}{m_1}\hat{u}_1\,(m_1,m_2,\mathbf{J})\,, \quad m_1 \neq 0\ . \tag{6.4}$$

Although this condition was not built into our determination of $\mathbf{u}$, it is nevertheless well satisfied. Of all the components of $\hat{u}_2$, we can discard all but $\hat{u}_2(0,m_2,\mathbf{J}), m_2 > 0$, using $\hat{u}_1$ and the reality condition to find the others. It is interesting that the torus fitting method of Section 4 fails if one attempts to introduce the constraints (6.4) at the start. This circumstance can be understood analytically by analyzing Eq. (4.9) under the constraint.

The cost of evaluating the Fourier coefficients by spline interpolation goes up sharply with the number of mesh points $\mathbf{J}_i$. For that reason we avoid the full

5×5 mesh for extensive calculations, and instead do calculations in each of four overlapping squares, each based on the 3×3 mesh in one corner of Ω. The squares are denoted by $\Omega_i, i = 1, \cdots, 4$; each one extends 5% in each direction beyond the square formed by mesh points. They are numbered as follows: Ω_1, lower left; Ω_2, lower right; Ω_3; upper left; Ω_4; upper right. On a 3×3 mesh the spline scheme reduces to interpolation by single quadratic polynomials. We notice no decrease in accuracy from using the quadratic rather than piece-wise cubic scheme.

For increments of $\mathbf{J}$ in N_0 turns we adopt the notation

$$\mathbf{J}' - \mathbf{J} = \mathcal{D}(\mathbf{J}, \mathbf{\Phi}, N_0) \tag{6.5}$$

To get an impression of the problems involved in bounding $\mathcal{D}$, we first plot $\mathcal{D}$ as a function of one of its four arguments, with the others held fixed. In Figure 12 we show a result for $\mathbf{\Phi}$ dependence, plotting $\mathcal{D}_1(\mathbf{J}, \mathbf{\Phi}, 1)$ versus $\mathbf{\Phi}_1$ for $\mathbf{\Phi}_2 = 0$ and $\mathbf{J} = (2.55, 1.525) \cdot 10^{-6} m$. In Figure 13 we show $\mathbf{J}$ dependence, plotting $\mathcal{D}_1(\mathbf{J}, \mathbf{\Phi}, 1)$ versus J_1 at $J_2 = 1.525 \cdot 10^{-6} m$ with $\mathbf{\Phi} = 0$. Doing a number of such plots, for various values of N_0, we encounter a wide variety of functional forms, but in every case there are many oscillations in the $\mathbf{\Phi}$ dependence, but only one or two in the $\mathbf{J}$ dependence ($\mathbf{J}$ being restricted to one of the four squares). Thus, it appears that we may need to sample only a small number of $\mathbf{J}$ values, but many $\mathbf{\Phi}$ values at each $\mathbf{J}$. We therefore start by trying to get information of a statistical sort on the required number of $\mathbf{\Phi}$ samples at fixed $\mathbf{J}$. At fixed $\mathbf{J}$ we evaluate $\mathcal{D}$ on random sequences of points in the $\mathbf{\Phi}$ plane.

n_s	n_p	$< d_1 >$	$< d_2 >$	σ_1	σ_2	$\min(d_1)$	$\max(d_1)$	$\min\ (d_2)$	$\max\ (d_2)$
200	50	$7.1{\cdot}10^{-13}$	$1.8{\cdot}10^{-12}$	$9.7{\cdot}10^{-14}$	$1.2{\cdot}10^{-12}$	$5.1{\cdot}10^{-13}$	$9.7{\cdot}10^{-13}$	$5.6{\cdot}10^{-13}$	$2.2{\cdot}10^{-12}$
100	100	$7.5{\cdot}10^{-13}$	$1.9{\cdot}10^{-12}$	$9.0{\cdot}10^{-14}$	$1.7{\cdot}10^{-13}$	$5.8{\cdot}10^{-13}$	$9.7{\cdot}10^{-13}$	$1.4{\cdot}10^{-12}$	$2.3{\cdot}10^{-12}$
10	1000	$8.9{\cdot}10^{-13}$	$2.2{\cdot}10^{-12}$	$5.7{\cdot}10^{-14}$	$1.1{\cdot}10^{-13}$	$8.2{\cdot}10^{-13}$	$1.0{\cdot}10^{-12}$	$1.9\ {\cdot}10^{-12}$	$2.3{\cdot}10^{-12}$

Table 1: Statistical data on the quantities d_k defined in Eq. (6.6), for $N_o = 10$. The ensemble average $< d_k >$, standard deviation σ_k, and minima and maxima refer to an ensemble of n_s values of d_k, each member of the ensemble coming from a maximum over n_p values of $\mathbf{\Phi}$ at $\mathbf{J} = (2.55, 1.525)\ {\cdot}10^{-6}$ m.

In Table 1 we show results for n_s different sequences of n_p points each, for various choices of n_s and n_p at $N_o = 10$. For sequence number j we find the maximum,

$$d_k^{(j)} = \max_{1 \le \mathrm{i} \le \mathrm{n_p}} \left| \mathcal{D}_k \left(\mathbf{J}, \mathbf{\Phi}_i^{(j)}, N_o \right) \right| \ , \quad k = 1, 2 \ , \tag{6.6}$$

and compute the mean, minimum, maximum, and standard deviation of $d_k^{(j)}$ with respect to j. There is a total of 10000 samples for each line of the table, different samples from one line to the next. It appears that 10000 samples are enough to determine the maximum of the function to a few percent. That is indicated by one- dimensional plots such as Figure 10, and also by the fact that three different maxima over 10000 are almost the same. Fortunately, we also see that 100 samples are enough to get an estimate which is adequate for our purposes. For sequences of length $n_p = 100$, the standard deviation of $d_k^{(j)}$ over 100 sequences is about 10% of the mean, and the maximum $d_k^{(j)}$ is only about 60% larger than the minimum

$d_k^{(j)}$. Very similar results were obtained at several other values of $\mathbf{J}$ and N_o. The picture that emerges may be described as rapid oscillatory behavior in $\mathbf{\Phi}$ that is statistically the same at all $\mathbf{J}$ and N_o.

It now seems reasonable to explore the $\mathbf{J}$ dependence of

$$d_k(\mathbf{J}) = \max_{1 \le i \le n_p} |\mathcal{D}_k(\mathbf{J}, \mathbf{\Phi}_i, N_o)| \ , \quad k = 1, 2 \ , \tag{6.7}$$

taking at each $\mathbf{J}$ a different random sequence $\{\mathbf{\Phi}_i\}$ of small fixed length, say $n_p = 100$. The $d_k(\mathbf{J})$ are expected to be smallest at the mesh points $\{\mathbf{J}_i\}$ corresponding to the original fitted tori. We might look for larger values at the following points in the $\mathbf{J}$ plane:

(i) Points near resonances, especially points where resonance lines cross.

(ii) Points a maximum distance from mesh points, where there could be interpolation error.

(iii) Points near the boundary of Ω, where there could be interpolation error and also effects of resonances lying outside Ω but close enough to be felt.

In practice we check such points, but also do random sampling in both $\mathbf{J}$ and $\mathbf{\Phi}$ at once. In choosing the number of samples for the latter we are informed by the above discussion of $\mathbf{\Phi}$ sampling. In a region where the $\mathbf{J}$ variation of $\mathcal{D}$ is expected to be small (expected, for example, on the basis of one-dimensional plots such as Figure 11) the number of samples in $(\mathbf{J}, \mathbf{\Phi})$ space should be about the same as the number of $\mathbf{\Phi}$ samples at fixed $\mathbf{J}$, about 100 in the present example. Since we think that $\mathcal{D}$ has small variation over one cell of our $\mathbf{J}$ mesh, this means 1600 points for the 16-cell mesh of Figure 5. This guess is confirmed by a statistical study of sampling in $\mathbf{J}$ and $\mathbf{\Phi}$ at once, for small N_o. With n_p samples of $(\mathbf{J}, \mathbf{\Phi})$ in a 4-cell

region, we found that the standard deviations of maxima over n_s sequences were 10 to 15% of mean values, for $N_o = 1, 10, 100$, with $n_p = 400$ and $n_s = 15$.

For a first exploration we have found sampling in $\mathbf{J}$ and $\mathbf{\Phi}$ at once to be the most workable scheme. It is aided by a simple graphical device: we store all values of $|\mathcal{D}_k|$, and then plot in the (J_1, J_2) plane all $\mathbf{J}$ such that $|\mathcal{D}_k|$ is larger than half its maximum value. This sometimes reveals small domains of large $|\mathcal{D}_k|$ that may often be eliminated by introducing more mesh points. In the region Ω considered here, no additional mesh points were needed; the values of $|\mathcal{D}_k|$ larger than half-maximum are distributed rather uniformly over the region. In particular, values on resonances lines and at the point where six resonances cross were not larger than average. Furthermore, the values on the original fitted tori were not much smaller than average. Apparently, the resonances in this region are so narrow that motion on a resonance closely follows a neighboring torus.

N_0	$\max\|\mathcal{D}_1\|$	$\max\|\mathcal{D}_2\|$	$<\|\mathcal{D}_1\|>$	$<\|\mathcal{D}_2\|>$	$<\mathcal{D}_1>$	$<\mathcal{D}_2>$
1	$9.9{\cdot}10^{-13}$	$1.9{\cdot}10^{-12}$	$2.4{\cdot}10^{-13}$	$4.7{\cdot}10^{-13}$	$3.8{\cdot}10^{-15}$	$-6.4{\cdot}10^{-15}$
10	$1.5{\cdot}10^{-12}$	$1.7{\cdot}10^{-12}$	$2.7{\cdot}10^{-13}$	$4.7{\cdot}10^{-13}$	$2.1{\cdot}10^{-15}$	$3.8{\cdot}10^{-14}$
100	$1.2{\cdot}10^{-12}$	$2.5{\cdot}10^{-12}$	$3.1{\cdot}10^{-13}$	$5.4{\cdot}10^{-13}$	$-2.7{\cdot}10^{-14}$	$-2.0{\cdot}10^{-14}$
1000	$1.5{\cdot}10^{-12}$	$2.7{\cdot}10^{-12}$	$3.3{\cdot}10^{-13}$	$5.2{\cdot}10^{-14}$	$1.3\cdot10^{-14}$	$2.7\cdot10^{-14}$
10000	$1.9{\cdot}10^{-12}$	$2.7{\cdot}10^{-12}$	$4.0{\cdot}10^{-13}$	$6.5{\cdot}10^{-13}$	$1.0{\cdot}10^{-14}$	$3.9{\cdot}10^{-14}$

Table 2: Data on $\mathbf{J}' - \mathbf{J} = \mathcal{D}(\mathbf{J}, \mathbf{\Phi}, N_0)$, the change of $\mathbf{J}$ in N_0 turns, for 400 random samples of $(\mathbf{J}, \mathbf{\Phi})$ with $\mathbf{J}$ in subregion Ω_4. The brackets $<>$ indicate ensemble averages.

In Table 2 we show results from 400 samples of $(\mathbf{J}, \mathbf{\Phi})$ in Ω_4, for N_0 ranging from 1 to 10000. Similar results were obtained in the other three Ω_i. In addition to the ensemble maxima of $|\mathcal{D}_k|$, we also give the ensemble average $<|\mathcal{D}_k|>$ of the absolute values, and the ensemble average $<\mathcal{D}_k>$ including sign. The results are remarkably independent of N_0. A trajectory starting on a torus is as close to that torus after 10000 turns as it is after 1 turn. Furthermore, averages including sign are very small, of order 10^{-14}m, which indicates that the orbit makes small oscillations about the torus, spending almost as much time on one side as on the other. In some average sense, the tori are invariant to much greater precision than the maximum deviations would indicate.

In Table 3 we show data on $\mathcal{D}$ for $N_0 = 10000$ for each of the four squares, again for 400 samples of $(\mathbf{J}, \mathbf{\Phi})$ in each square. Our statistical study of sampling for $N_0 = 1$, 10, 100 indicates that the values of $\max|\mathcal{D}_k|$ should be increased by

about 30% to estimate the true maxima of the functions. It therefore seems safe to increase them by 50%, which leads to the following estimates of maxima over Ω:

$$\begin{aligned} (\delta J_1, \delta J_2) &= (2.8, 4.0) \cdot 10^{-12} m, \\ \delta J_k &= \sup_{\mathbf{J}, \mathbf{\Phi} \in \Omega} |\mathcal{D}_k(\mathbf{J}, \mathbf{\Phi}, 10000)| \end{aligned} \tag{6.8}$$

Region	$\max\lvert\mathcal{D}_1\rvert$	$\max\lvert\mathcal{D}_2\rvert$	$<\lvert\mathcal{D}_1\rvert>$	$<\lvert\mathcal{D}_2\rvert>$	$<\mathcal{D}_1>$	$<\mathcal{D}_2>$
Ω_1	$1.5{\cdot}10^{-12}$	$2.1{\cdot}10^{-12}$	$3.1{\cdot}10^{-13}$	$4.3{\cdot}10^{-13}$	$1.5{\cdot}10^{-14}$	$-2.3{\cdot}10^{-14}$
Ω_2	$1.2{\cdot}10^{-12}$	$2.6{\cdot}10^{-12}$	$3.5{\cdot}10^{-13}$	$6.3{\cdot}10^{-13}$	$-2.2{\cdot}10^{-15}$	$1.0{\cdot}10^{-14}$
Ω_3	$1.4{\cdot}10^{-12}$	$1.6{\cdot}10^{-12}$	$3.1{\cdot}10^{-13}$	$4.4{\cdot}10^{-13}$	$-1.2{\cdot}10^{-14}$	$-3.4{\cdot}10^{-14}$
Ω_4	$1.9{\cdot}10^{-12}$	$2.7{\cdot}10^{-12}$	$4.0{\cdot}10^{-13}$	$6.5{\cdot}10^{-13}$	$1.0{\cdot}10^{-14}$	$3.9{\cdot}10^{-14}$

Table 3: Data on $\mathbf{J}' - \mathbf{J} = \mathcal{D}(\mathbf{J}, \mathbf{\Phi}, 10000)$, the change in $\mathbf{J}$ over 10000 turns, for 400 random samples of $(\mathbf{J}, \mathbf{\Phi})$ in each subregion Ω_i. The brackets <> indicate ensemble averages.

We can now follow the argument of Section 3 to get a long-term bound on the motion. To get a bound for 10^8 turns from our results for 10^4 turns, we take a rectangular region $\Omega_0 \subset \Omega$ such that $\Delta J_i / \delta J_i = 10^4$, where the ΔJ_i are the widths of the strips forming the annulus between Ω_0 and Ω. Thus, Ω_0 is the region

$$\begin{aligned} 2.54 \cdot 10^{-6}\mathrm{m} < J_1 < 2.79 \cdot 10^{-6}\mathrm{m}\,, \\ 1.38 \cdot 10^{-6}\mathrm{m} < J_2 < 1.60 \cdot 10^{-6}\mathrm{m}\,. \end{aligned} \tag{6.9}$$

Any trajectory beginning in Ω_0 will stay within the boundaries of the bigger region Ω, defined in (6.1), for at least 10^8 turns.

7. VARIATION OF J NEAR A STRONG RESONANCE

We examined a number of regions in phase space that were similar to the region studied in Section 6 with respect to size and degree of nonlinearity. In most regions the variations of **J** were similar in magnitude to those found above, but in some cases much larger variations were found, due to the presence of relatively broad resonances.

As an example we investigate a region Ω_r:

$$\begin{aligned} 2.235 \cdot 10^{-6}\mathrm{m} < J_1 < 2.456 \cdot 10^{-6}\mathrm{m} \ , \\ 1.277 \cdot 10^{-6}\mathrm{m} < J_2 < 1.303 \cdot 10^{-6}\mathrm{m} \ . \end{aligned} \tag{7.1}$$

The [5,6] resonance appearing in Figure 10 passes through the middle of Ω_r. In a broad band about the [5,6] line, the torus fitting program fails. It succeeds easily, however, if the mesh points $\{\mathbf{J}_i\}$ are placed at a distance of $5{\cdot}10^{-8}$m from the line. Keeping mesh points at about that distance, we set up a 4×3 mesh which provides a definition of $\mathbf{u}(\mathbf{J}, \mathbf{\Phi})$ throughout Ω_r. This definition is somewhat arbitrary, depending strongly on the choice of mesh points. If we take the mesh points as close to the resonance as we possibly can, then the **J** dependence of $\mathbf{u}(\mathbf{J}, \mathbf{\Phi})$ does not look sensible, and varies erratically with the choice of mesh points. This is comprehensible by analogy with a system in one lower dimension (1-1/2 degrees of freedom). If we tried to interpolate two families of invariant curves $I(J, \phi)$, one on either side of a broad island chain, we would get nonsense if those curves were too close to the separatrix. The two sides of the separatrix are out of phase, one having a maximum and the other a minimum at a given point, and they have a cusp where they touch. Our functions have too simple a **J** dependence to follow first one half of the separatrix, then have some reasonable form inside

the islands, then follow the other half of the separatrix, as $\mathbf{J}$ is varied across the resonance value.

Having made a definite choice of the change of variable, $\mathbf{I} = \mathbf{J} + \mathbf{u}(\mathbf{J}, \mathbf{\Phi})$, however arbitrary, it is interesting to see how $\mathbf{J}$ evolves in time. In the work of the preceeding section, $\mathbf{J}$ took small, seemingly random steps of order 10^{-12} m. By contrast, near the [5,6] resonance it follows a straight line segment with slope 6/5 in the (J_1, J_2) plane, with excursions of up to 10^{-8}m, as shown in Figure 14. This suggests that the motion of $\mathbf{J}$ follows the isolated resonance model.

The isolated resonance model is described by the Hamiltonian

$$H_r = A(\mathbf{J}) + B(\mathbf{J}) \cos(\mathrm{m} \cdot \mathbf{\Psi} - \mathrm{n}\theta + \mathrm{C}(\mathbf{J})) \ , \tag{7.2}$$

which depends on only one angular coordinate,

$$\mathbf{m} \cdot \mathbf{\Psi} - n\theta \ .$$

It is useful to make a canonical transformation,

$$\begin{aligned}
\xi_1 &= \frac{1}{\|\mathbf{m}\|} (m_1\psi_1 + m_2\psi_2 - n\theta) \ , \\
\xi_2 &= \frac{1}{\|\mathbf{m}\|} (m_2\psi_1 - m_1\psi_2) \ , \\
K_1 &= \frac{1}{\|\mathbf{m}\|} (m_1 J_1 + m_2 J_2) \ , \\
K_2 &= \frac{1}{\|\mathbf{m}\|} (m_2 J_1 - m_1 J_2) \ , \\
\|\mathbf{m}\| &= \left[m_1^2 + m_2^2\right]^{1/2} \ .
\end{aligned} \tag{7.3}$$

This arises from the generator

$$F_2(\mathbf{K}, \mathbf{\Psi}) = \boldsymbol{\xi} \cdot \mathbf{K} \ . \tag{7.4}$$

The new Hamiltonian is the same as (7.2), except for addition of the term $\partial F_2/\partial\theta = -nK_1/\|m\|$. Since H_r is independent of ξ_2, the conjugate action K_2 is constant. With K_2 constant the new Hamiltonian depends only on K_1 and ξ_1, and is therefore itself constant.

If we identify $\mathbf{J}$ and $\mathbf{\Psi}$ of (7.2) with our new variables defined through the complete canonical transformation (2.26), then we expect $\mathbf{J}$ to move on a straight line segment, K_2 = constant, as in Figure 14. In general such motion could be unstable, but in the present case it is stable over a long time and the motion of K_1 resembles that of a physical pendulum. To see a phase portrait of the pendulum motion, we plot $K_1 = \mathbf{m}\cdot\mathbf{J}/\|m\|$ versus $\mathbf{m}\cdot\mathbf{\Psi}$ (mod 2π), taking values of $(\mathbf{J},\mathbf{\Phi})$ on our usual surface of section from the N_0 turn map. Results are shown in Figure 15. We seem to have cleanly defined curves, in spite of the somewhat arbitrary choice of $\mathbf{u}(\mathbf{J},\mathbf{\Phi})$.

The variable K_2, whether plotted as a function of ξ_2 or plotted versus turn number, shows random variation with a scatter of about 10^{-11}m. Thus the variation of $\mathbf{J}$ in the direction of the vector $(-m_2,m_1)$ is small. The variation in the perpendicular direction (m_1,m_2) is large but oscillatory. The question arises as to whether there is any long-term drift of the center of oscillation in the (m_1,m_2) direction. Judging from a few thousand turns, the rotation curves of K_1 in Figure 15 (the curves that correspond to the pendulum swinging all the way around) are defined to about 10^{-11} m; one sees that much scatter in a magnified graphical display. Thus, drift of the center of oscillation in either direction, $(-m_2,m_1)$ or (m_1,m_2), seems to be limited to about 10^{-11} m over N_0 turns, with N_0 a few thousand. This is not much bigger than the drift of $\mathbf{J}$ itself observed in the region of Section 6.

To handle this problem more formally, one should treat the rotation curves of K_1 in the same way that we treated the tori followed by **I**. Using a one-dimensional version of the torus fitting program, one should construct a few curves fitted to data on K_1, and interpolate those curves to get a continuous family of curves labeled by $\mathcal{J} =< K_1 >$, the average over ξ_1. As in our previous work, $\mathcal{J}$ would be regarded as a new, nearly constant variable, and examination of its variation would lead to limits on the oscillation of K_1, just as we previously found limits on the oscillation of **I** by controlling the variation of **J**.

8. CONCLUSIONS AND OUTLOOK

We have demonstrated a technique for setting bounds on nonlinear Hamiltonian motion for a finite but very long time. We gave a nontrivial example in 2 1/2 degrees of freedom, an example in which the existence of invariant tori does not guarantee stability for infinite time. Stability for a finite time can be ensured, in spite of the existence of nonlinear resonances, chaotic motion, and Arnol'd Diffusion.

Finite-time bounds follow from the existence of a continuous family of approximate invariant tori. We have described an efficient numerical method for the construction of such a family, which provides a canonical transformation to new action-angle variables such that the action is nearly constant. The transformation is mathematically well-defined, despite its numerical provenance. Conclusions about stability would be rigorous if one could find a bound on the variation of the new action $\mathbf{J}$ over N_o turns. The variation $\mathcal{D}(\mathbf{J}, \mathbf{\Phi}_o, N_o)$ of $\mathbf{J}$ from any initial condition $(\mathbf{J}, \mathbf{\Phi})$ can be computed with adequate accuracy. The only serious uncertainty arises in bounding the maximum of the variation over all initial conditions in an open region. We have constructed a tentative bound, that we find convincing, by a statistical study of randomly chosen initial conditions. We have also tested particular initial conditions, for instance points on resonances, that might be expected to produce large variations. Of course, the uncertainty can be reduced by expending more computer time, but it may also be possible to do sampling in more informative ways. For instance, it may be interesting to make a Fourier analysis of the $\mathbf{\Phi}$ dependence of $\mathcal{D}$, and try to correlate behavior of Fourier amplitudes with resonances. One might also try to estimate a bound on the derivative of $\mathcal{D}$ with

respect to **J**, again looking for correlations of large derivatives with resonances. Further work should explore these possibilities, among others.

A large part of the power of the present analysis derives from studying the variation of **J** over a large number N_o of turns. By carefully integrating the equations of motion for N_o turns, we account for cancellations that occur in typical stable motion and prevent accrual of large increments of **J**. On the other hand, N_o need not be so large as to create problems of round-off error. Rounding error is firmly under control in this approach, even when we seek bounds for the very long storage times typical of proton storage rings.

One is strongly motivated to extend the calculations to 3 1/2 degrees of freedom, since motion in a third coordinate associated with oscillations in energy (synchrotron oscillations) is known to have an important influence in long-term stability of accelerators. It is also interesting to study the beam-beam interaction in colliding-beam machines, which may induce a somewhat different pattern of nonlinear resonances. Both of these problems are being pursued.

Finally, we express the hope that our experience in efficient treatment of several degrees of freedom may find application in other fields, such as semi-classical quantum theory and plasma theory. Since our scheme for approximating invariant tori requires only the Poincaré map of the system, it can be applied directly to almost any problem in a few degrees of freedom.

APPENDIX A

Our model for motion transverse to the beam in an accelerator is based on a Hamiltonian of the form[1,2,3]

$$H(\mathbf{I}, \mathbf{\Phi}, s) = \mathbf{\Omega}(s) \cdot \mathbf{I} + V(\mathbf{I}, \mathbf{\Phi}, s) \quad , \tag{A.1}$$

where the independent variable s is arc length along a closed reference orbit, and $\mathbf{\Omega}(s) = (1/\beta_1(s), (1/\beta_2(s))$, is formed from the Courant-Snyder functions $\beta_i(s)$ which characterize the linear features of the magnet lattice. The nonlinear perturbation V comes from sextupole magnets, and has the form

$$V(\mathbf{I}, \mathbf{\Phi}, s) = \frac{S(s)}{3!}\left(x_1^3 - 3x_1x_2^2\right) \quad , \tag{A.2}$$

where x_1 and x_2 are horizontal and vertical displacements of the particle from the reference orbit. These displacements are given in terms of the action-angle coordinates by the equation

$$x_i = [2I_i\beta_i(s)]^{1/2}\cos\Phi_{\mathrm{i}} \quad , \quad \mathrm{i} = 1, 2 \quad . \tag{A.3}$$

The function $S(s)$ is zero except over the extent of a sextupole magnet where it is constant, with the value S_i at the i-th magnet. Both $S(s)$ and $\beta_i(s)$ are periodic with period C, the length of the reference orbit.

The Hamiltonian may be put into the form (2.1) by a canonical transform designed to remove the s-dependence of the linear term. The generator of the transformation $(\mathbf{I}, \mathbf{\Phi}) \rightarrow (\mathbf{I}', \mathbf{\Phi}')$ is

$$F_2\left(\mathbf{I}', \mathbf{\Phi}, s\right) = \mathbf{I}' \cdot \left[\mathbf{\Phi} + \frac{\nu_0 s}{R} - \int_0^s \mathbf{\Omega}(u)du\right] \quad , \tag{A.4}$$

where $2\pi R = C$ and

$$\boldsymbol{\nu}_0 = \frac{1}{2\pi}\int_0^C \boldsymbol{\Omega}(u)du \ . \tag{A.5}$$

This yields

$$\mathbf{I} = \frac{\partial F_2}{\partial \boldsymbol{\Phi}} = \mathbf{I}' \ , \tag{A.6}$$

$$\boldsymbol{\Phi}' = \frac{\partial F_2}{\partial \mathbf{I}'} = \boldsymbol{\Phi} + \frac{s}{R}\boldsymbol{\nu}_0 - \int_0^s \boldsymbol{\Omega}(u)du \ . \tag{A.7}$$

$$\begin{aligned} H' &= H + \frac{\partial F_2}{\partial s} \\ &= \frac{1}{R}\boldsymbol{\nu}\cdot\mathbf{I}' + V\left(\mathbf{I}', \boldsymbol{\Phi}' + \int_0^s \boldsymbol{\Omega}(u)du - \boldsymbol{\nu}_0\frac{s}{R}\right) \ . \end{aligned} \tag{A.8}$$

The new Hamiltonian (A.8) has the form (2.1), after a change of independent variable $s \rightarrow \theta = s/R$. The linear term now represents harmonic motion.

Let us define

$$\boldsymbol{\chi}(s) = \int_0^s \boldsymbol{\Omega}(u)du \ , \tag{A.9}$$

$$\boldsymbol{\alpha} = -\frac{1}{2}\frac{d\boldsymbol{\beta}(s)}{ds} \tag{A.10}$$

Since $\boldsymbol{\beta}$ varies linearly over the extent of a sextupole magnet, we can compute $\boldsymbol{\chi}$ for use in (A.8) if we specify only the initial values of $\boldsymbol{\beta}, \boldsymbol{\alpha}$, and $\boldsymbol{\chi}$ at one edge of the magnet.

The parameters for the model that we study, one cell of an early design for the lattice of the Advanced Light Source at Lawrence Berkeley Laboratory, are given in Table IV. There are four sextupoles, each with leading edge located at s,

strength S, and length Δs. The values of $\boldsymbol{\beta}, \boldsymbol{\alpha}$, and $\boldsymbol{\chi}$ are for the leading edge. The units are meters for s and $\boldsymbol{\beta}$, (meters)$^{-3}$ for S. The total length of the cell is 16.4 m, and the unperturbed tunes are

$$\nu_{01} = 1.189735, \quad \nu_{02} = 0.681577 \ . \qquad (A.11)$$

Table IV: Berkeley ALS CELL.

s (Leading Edge)	$\beta_{1,2}$	$\alpha_{1,2}$	$\boldsymbol{\chi}_{1,2}$	S	Δs
5.775	1.4724	-1.7791	2.4799	-88.09	.20
	10.6957	8.4007	.8658		
6.875	3.9837	2.2722	2.8191	115.615	.20
	1.5798	.4167	1.2217		
9.325	3.1367	-1.9628	4.5996	115.615	.20
	1.4428	-.2681	2.9279		
10.425	2.2972	2.3448	4.8865	-88.09	.20
	7.6031	-7.0624	3.3945		

ACKNOWLEDGEMENTS

We thank John Irwin and Étienne Forest for many lively discussions and good suggestions. A seminar talk by Giorgio Turchetti aroused our interest in the Nekhoroshev Theorem and finite-time bounds.

REFERENCES

1. Physics of Particle Accelerators, AIP Conference Proceedings, No.153, Vol.1 and No.184, Vol.2, (Amer. Inst. Phys., New York, 1987 and 1989, resp.).
2. Nonlinear Dynamics Aspects of Particle Accelerators, Lecture Notes in Physics, Vol.247, (Springer, Berlin, 1986).
3. CERN Accelerator Schools, CERN reports 85-19 and 87-03 (CERN, Geneva, 1985 and 1987, resp.).
4. See the articles by Douglas and Forest in Ref. 1, by Wrulich and Iselin in Ref. 2, by Mais, Ripken, Wrulich, and Schmidt in Ref. 3.
5. V. I. Arnol'd, Mathematical Methods of Classical Mechanics (Springer, Berlin, 1978).
6. G. Gallavotti, The Elements of Mechanics (Springer, Berlin, 1983).
7. N. N. Nekhoroshev, Russian Math. Surveys 32:6 (1977) 1, translation of Uspekhi Mat. Nauk 32:6 (1977) 6.
8. G. Benettin, L. Galgani, and A. Giorgilli, Celestial Mechanics, 37 (1985) 1; G. Benettin and G. Gallavotti, J. Stat. Phys. 44 (1986) 293.
9. G. Gallavotti, in Critical Phenomena, Random Systems, and Gauge Theories, Les Houches 1984, Session XLIII, eds. K. Osterwalder and R. Stora (North-Holland, Amsterdam, 1985).
10. G. Benettin, in Nonlinear Evolution and Chaotic Phenomena, eds. G. Gallavotti and P. F. Zweifel (Plenum, New York, 1988).
11. A. Bazzani, S. Marmi, and G. Turchetti, "Nekhoroshev Estimate for Isochronous Non-resonant Symplectic Maps", University of Bologna report,

1990; G. Turchetti, in Number Theory and Physics, Springer Proceedings in Physics, Vol.47 (Springer, Berlin, 1990).

12. A. Giorgilli, A. Delsham Valdes, E. Fontich, E. Galgani, and C. Simo, J. Diff. Eq. 77 (1989) 167; A. Georgilli, in Proc. Workshop on Nonlinear Problems in Future Accelerators, Capri, Italy, April 19-25, 1990, eds. W. Scandale and G. Turchetti, (World Scientific, Singapore, 1991).

13. P. Lochak and A. Porzio, Ann. Inst. H. Poincaré, 51 (1989) 199.

14. B. V. Chirikov and V. V. Vecheslavov, "How Fast is the Arnol'd Diffusion?", Proc. Third Advanced ICFA Beam Dynamics Workshop: Beam-beam Effects in Circular Colliders, Novosibirsk, USSR, May 29 - June 3, 1989, eds. I. Koop and G. Tumaikin (Inst. Nuc. Phys., Novosibirsk, 1990); "KAM Integrability", preprint 88-110, (Inst. Nuc. Phys., Novosibirsk, 1988).

15. R. L. Warnock and R. D. Ruth, Proc. Third Advanced ICFA Beam Dynamics Workshop, *loc. cit.*, or SLAC-PUB-5020, June 1989.

16. R. L. Warnock and R. D. Ruth, Proc. Workshop on Nonlinear Problems in Future Particle Accelerators, *loc. cit.*, or SLAC-PUB-5304, July, 1990.

17. R. L. Warnock and R. D. Ruth, Phys. Rev. Lett. 66 (1991) 990.

18. R. L. Warnock and R. D. Ruth, Physica 26D (1987) 1.

19. W. E. Gabella, R. D. Ruth, and R. L. Warnock, *Second Advanced ICFA Beam Dynamics Workshop* , Lugano, 1988, CERN Report 88-04, or SLAC-PUB-4626.

20. R. L. Warnock, R. D. Ruth, and K. Ecklund, Proc. 1989 IEEE Particle Accelerator Conf., Chicago, March 20-23, 1989, eds. F. Bennett and J. Kopta, p.1325 (IEEE, New York, 1989).

21. W. E. Gabella, R. D. Ruth, and R. L. Warnock, Proc. U.S.-Japan Workshop on Nonlinear Dynamics and Particle Acceleration, Tsukuba, Japan, October 22-25, 1990, AIP Conference Proceedings, No.230, eds. Y. H. Ichikawa and T. Tajima (Amer. Inst. Phys., New York, 1991).

22. É. Forest, M. Berz, and J. Irwin, Part. Accel. 24 (1987) 91, and unpublished computer codes of Forest *et al.*.

23. S. Coffey, A. Deprit, É. Deprit, L. Healy, and B. R. Miller, Proc. of Conf. on Computer Aided Proofs in Analysis, Cincinnati, Ohio, March 1989, to be published in Inst. Math. and Appl. (Springer, Berlin).

24. R. L. Warnock, Phys. Rev. Lett. 66 (1991) 1803.

25. J. Pöschel, Comm. Pure. Appl. Math 35 (1982) 653.

26. L. Chierchia and G. Gallavotti, Nuovo Cimento B67 (1982) 277.

27. É. Forest and R. D. Ruth, Physica D 43 (1990) 105; R. D. Ruth, IEEE Trans. Nucl. Sci NS-30 (1983) 2669.

28. J. S. Berg and R. L. Warnock, SLAC-PUB-5458, to be published in Proc. 1991 Particle Accelerator Conf., San Francisco, May 6-9, 1991; R. L. Warnock, Proc. 1989 IEEE Particle Accelerator Conf., *loc. cit.* In Table 1 of this paper, the second entry in the second column should have exponent -7.

29. J. Irwin, Superconducting Super Collider report SSC-228, unpublished.

30. We thank V. Višnjić for emphasizing this point.

31. E. Isaacson and H. B. Keller, Analysis of Numerical Methods, (Wiley, New York, 1966); G. H. Golub and C. F. Van Loan, Matrix Computations, (Johns Hopkins U. Press, Baltimore, 1989).

32. C. de Boor, A Practical Guide to Splines, (Springer, Berlin, 1978).

FIGURE CAPTIONS

1. A commutative diagram showing how the maps $\mathcal{N}$ and $\mathcal{O}$ are induced by the original map $\mathcal{M}$ and changes of variable. The transformations $\mathcal{U}$ and $\mathcal{V}$ are given in explicit form through derivatives of the generator G.

2. A region $\mathcal{L}$ that forms a barrier to escape from $\mathcal{L}_0$ for at least N turns.

3. Values of $\mathbf{\Phi} = (\Phi_1, \Phi_2)$ at the surface of section $\theta = 0$ on an apparent invariant torus.

4. Values of $\mathbf{\Phi} = (\Phi_1, \Phi_2)$ at the surface of section $\theta = 0$ on a resonant orbit.

5. Three-dimensional plot of points (I_1, Φ_1, Φ_2) at the surface of section $\theta = 0$ on an apparent invariant torus. Example of Section 6 for $\mathbf{J}$ in the region specified in Eq.(6.1).

6. Three-dimensional plot of points (I_2, Φ_1, Φ_2) at the surface of section $\theta = 0$ on an apparent invariant torus. Example of Section 6 for $\mathbf{J}$ in the region specified in Eq.(6.1).

7. Resonant tune lines mapped into $\mathbf{J}$ space. All resonances in the region Ω with $|m_i| \leq 20$ are plotted. The points marked with an asterisk are the mesh points $\{\mathbf{J}_i\}$ corresponding to tori fitted to orbits.

8. The image in tune space of a rectangle in action space.

9. All resonances with $|m_i| \leq 20$ in a large region of $\mathbf{J}$ space.

10. All resonances with $|m_i| \leq 10$ in a large region of $\mathbf{J}$ space.

11. A test of accuracy of an high-order resonance line in $\mathbf{J}$ space. Following an orbit with initial condition on the [17, 16] line of Figure 7, we plot $[\Phi_1, \Phi_2]$ on a surface of section and find evidence of the expected resonance.

12. A plot of $J_1' - J_1 = \mathcal{D}_1(\mathbf{J}, \mathbf{\Phi}, 1)$ versus Φ_1 at $\Phi_2 = 0$ and $\mathbf{J} = (2.55, 1.525) \cdot 10^{-6}$m.

13. A plot of $J_1' - J_1 = \mathcal{D}_1(\mathbf{J}, \mathbf{\Phi}, 1)$ versus J_1 at $\mathbf{\Phi} = 0$ and $J_2 = 1.525 \cdot 10^{-6}$m.

14. Increments of $\mathbf{J}$ near a strong [5,6] resonance. The graph shows results from iteration of the 100 turn map, starting at $(\mathbf{J}_0, \mathbf{\Phi}_0)$, for fixed $\mathbf{J}_0$ and three different $\mathbf{\Phi}_0$. The points plotted are the increments $d\mathbf{J} = \mathbf{J} - \mathbf{J}_0$.

15. Phase portrait of the "pendulum" variables, $\mathbf{m} \cdot \mathbf{J}/\|\mathbf{m}\|$, $\mathbf{m} \cdot \mathbf{\Psi} (\mathrm{mod}\ 2\pi)$, near the [5, 6] resonance.

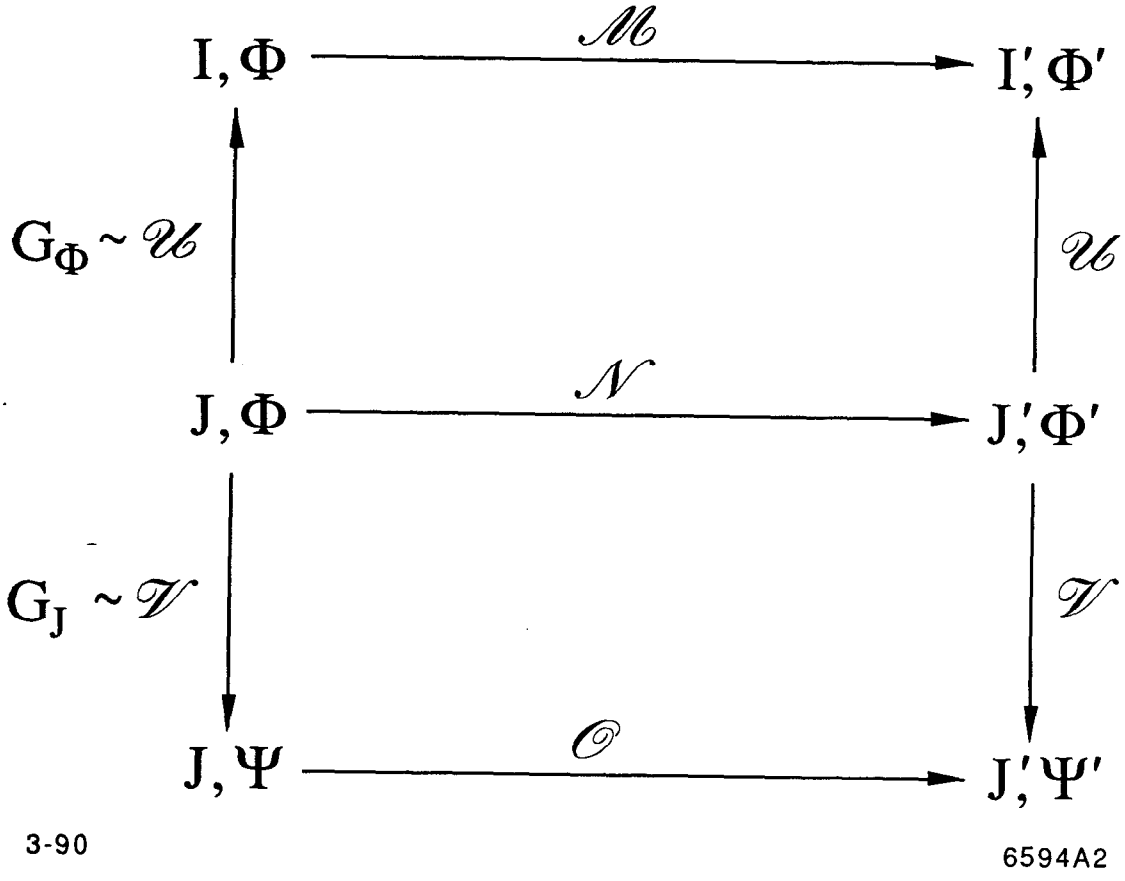

Fig. 1

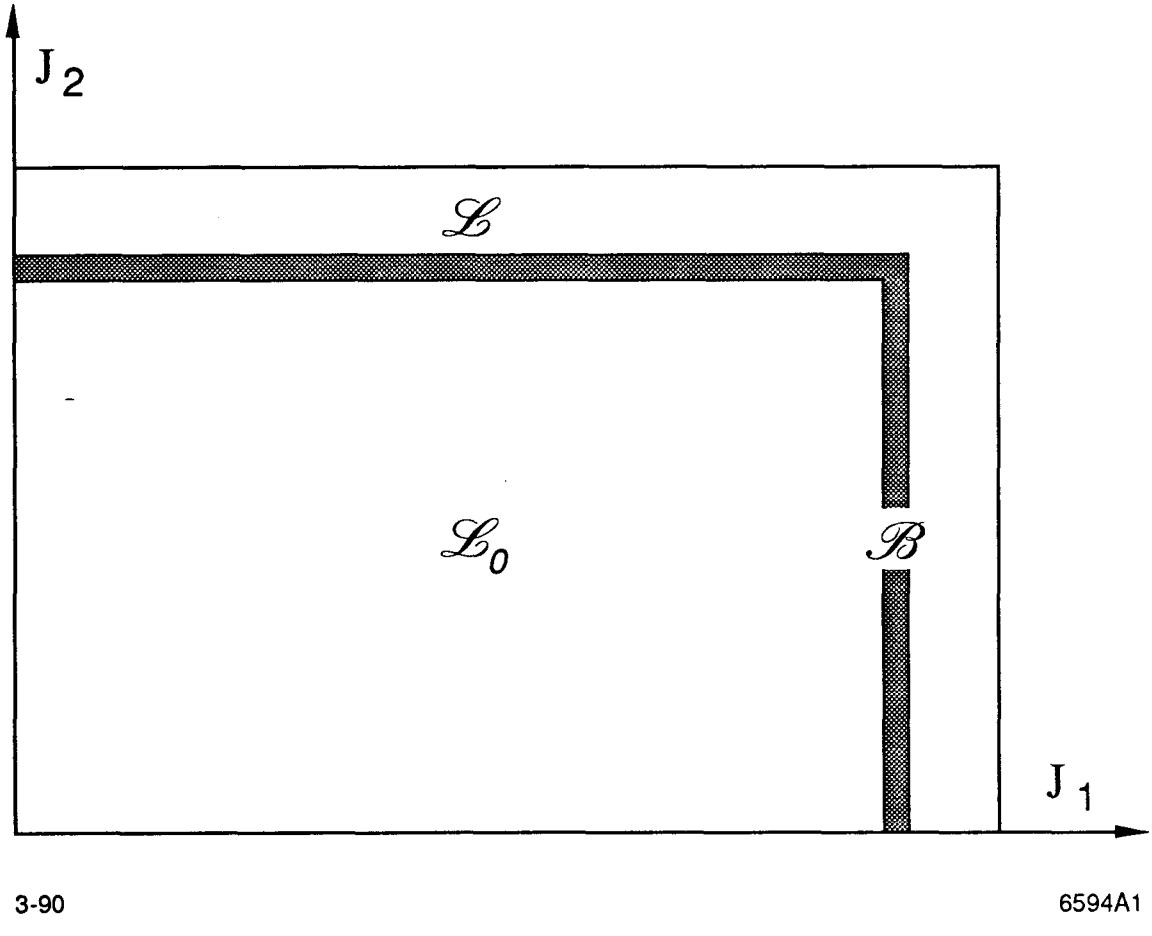

Fig. 2

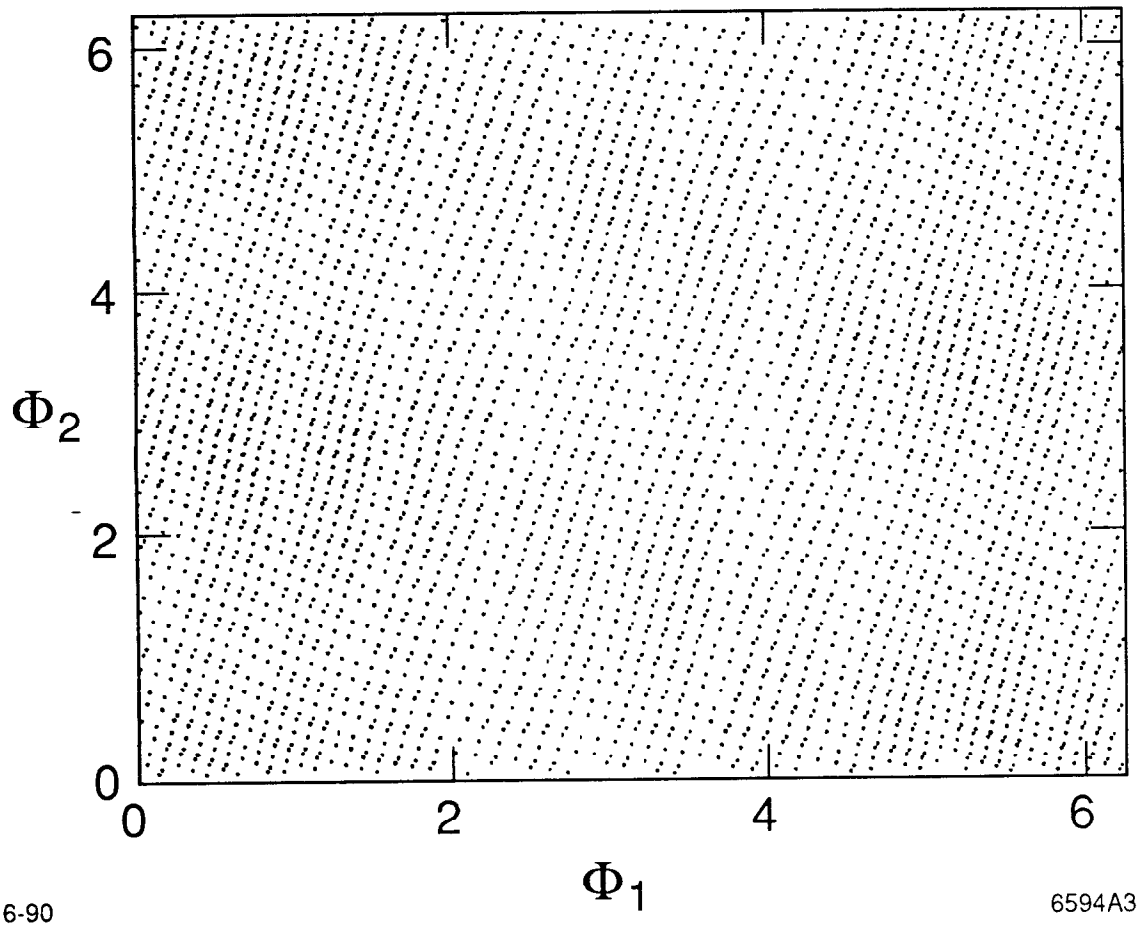

Fig. 3

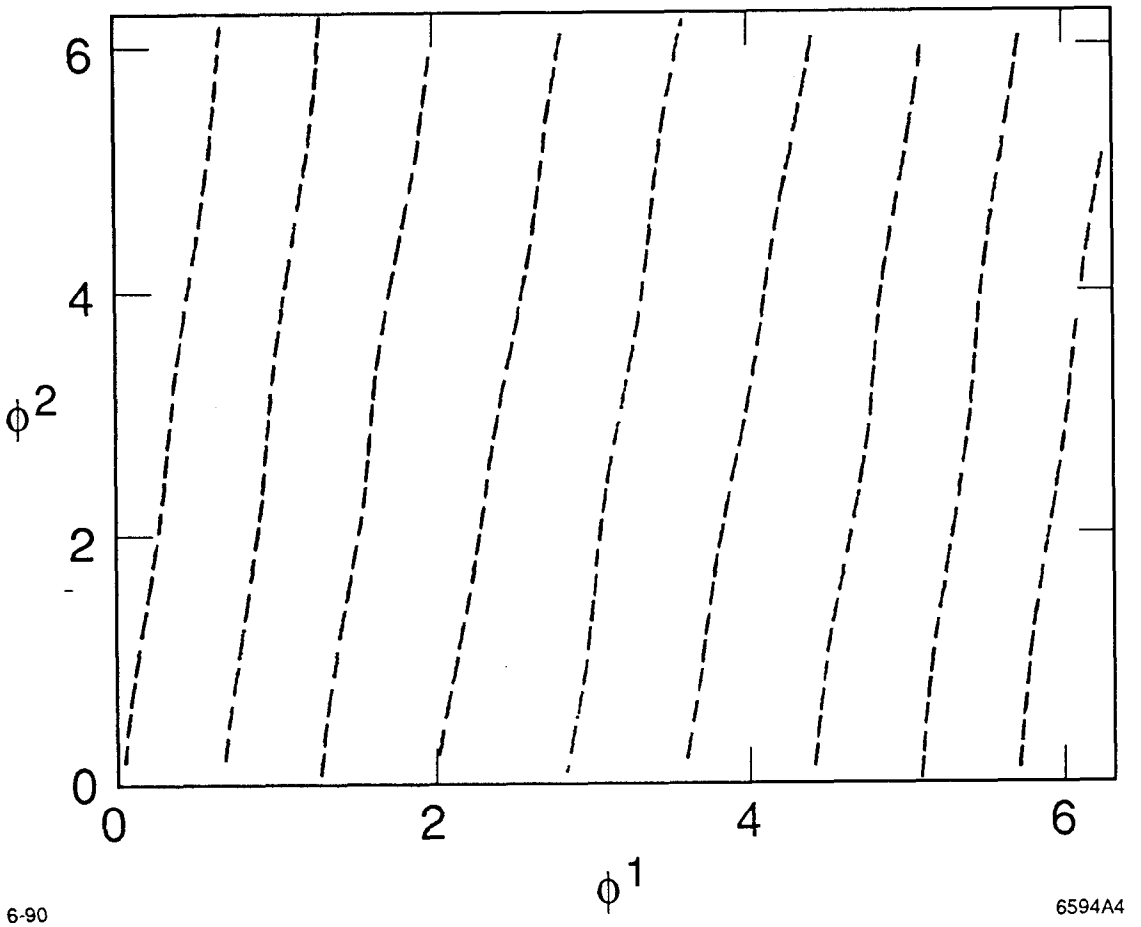

Fig. 4

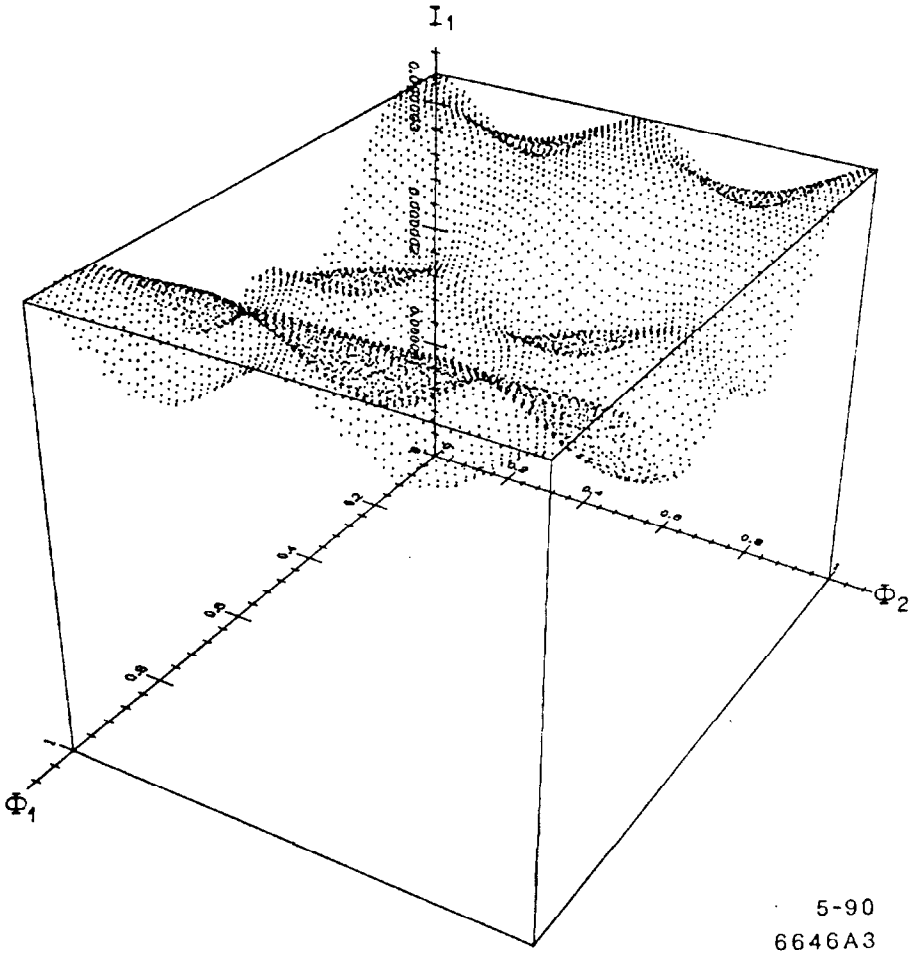

Fig. 5

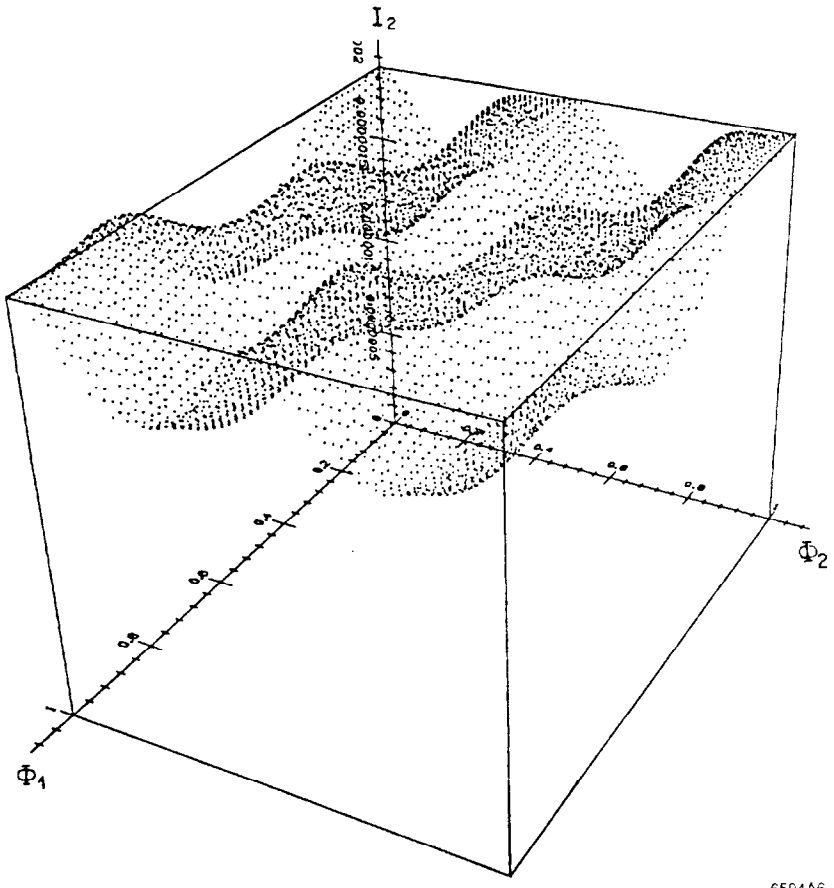

Fig. 6

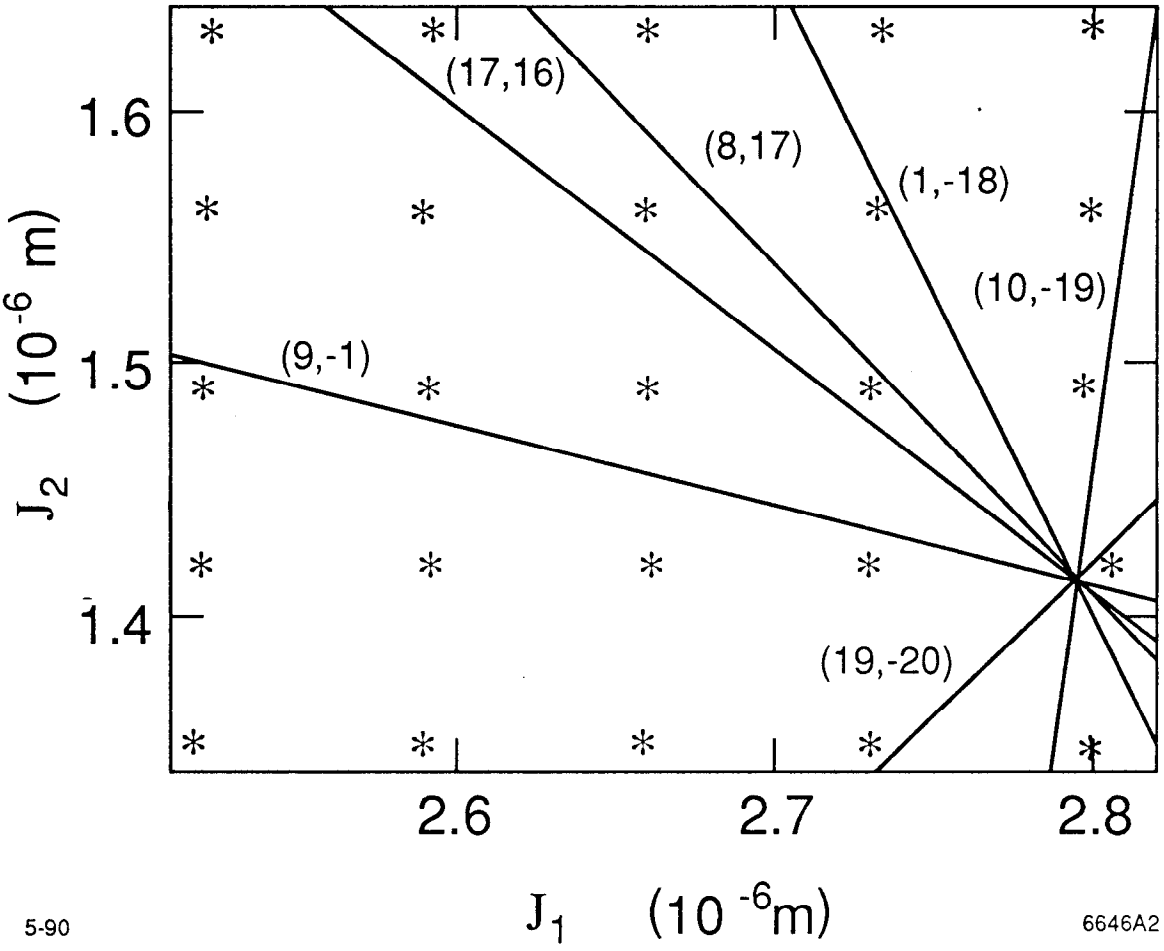
(17,16)
(8,17)
(1,-18)
(10,-19)
(9,-1)
(19,-20)
1.6
1.5
1.4
J_2 (10^{-6} m)
2.6
2.7
2.8
J_1 (10^{-6}m)
5-90
6646A2

Fig. 7

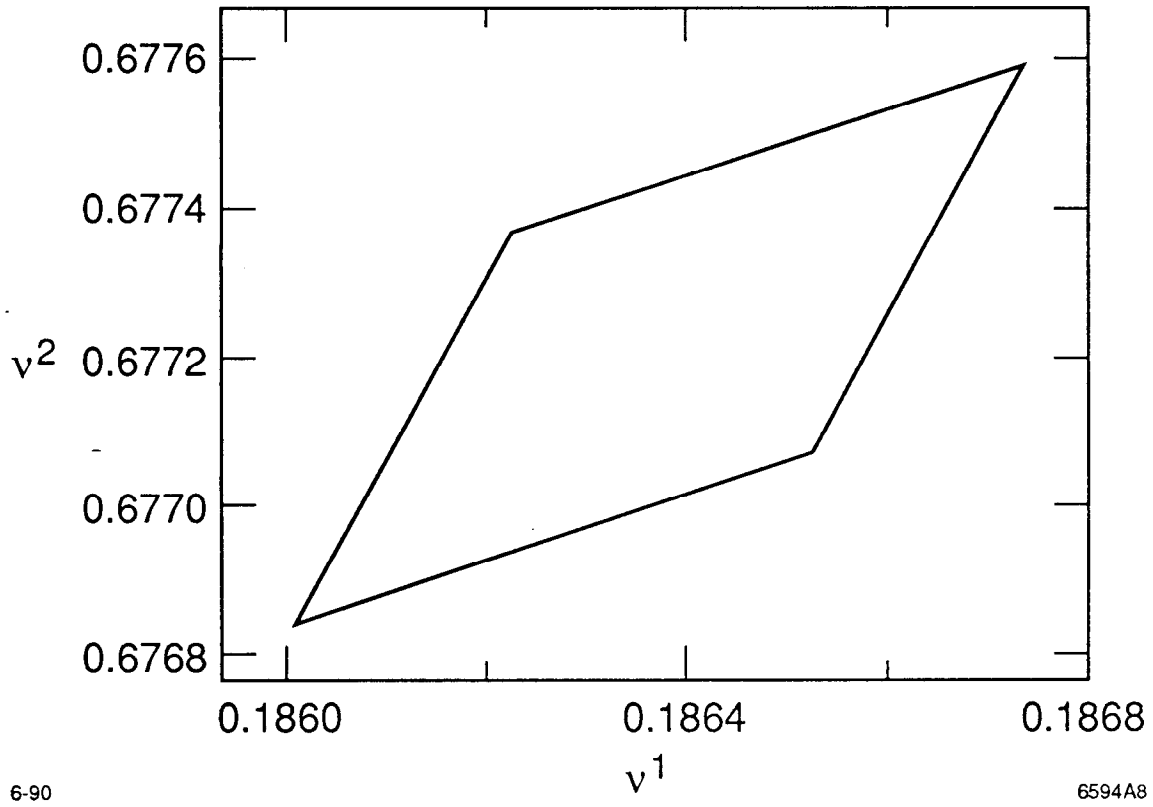
0.6776
0.6774
ν^2 0.6772
0.6770
0.6768
0.1860
0.1864
0.1868
ν^1
6-90
6594A8

Fig. 8

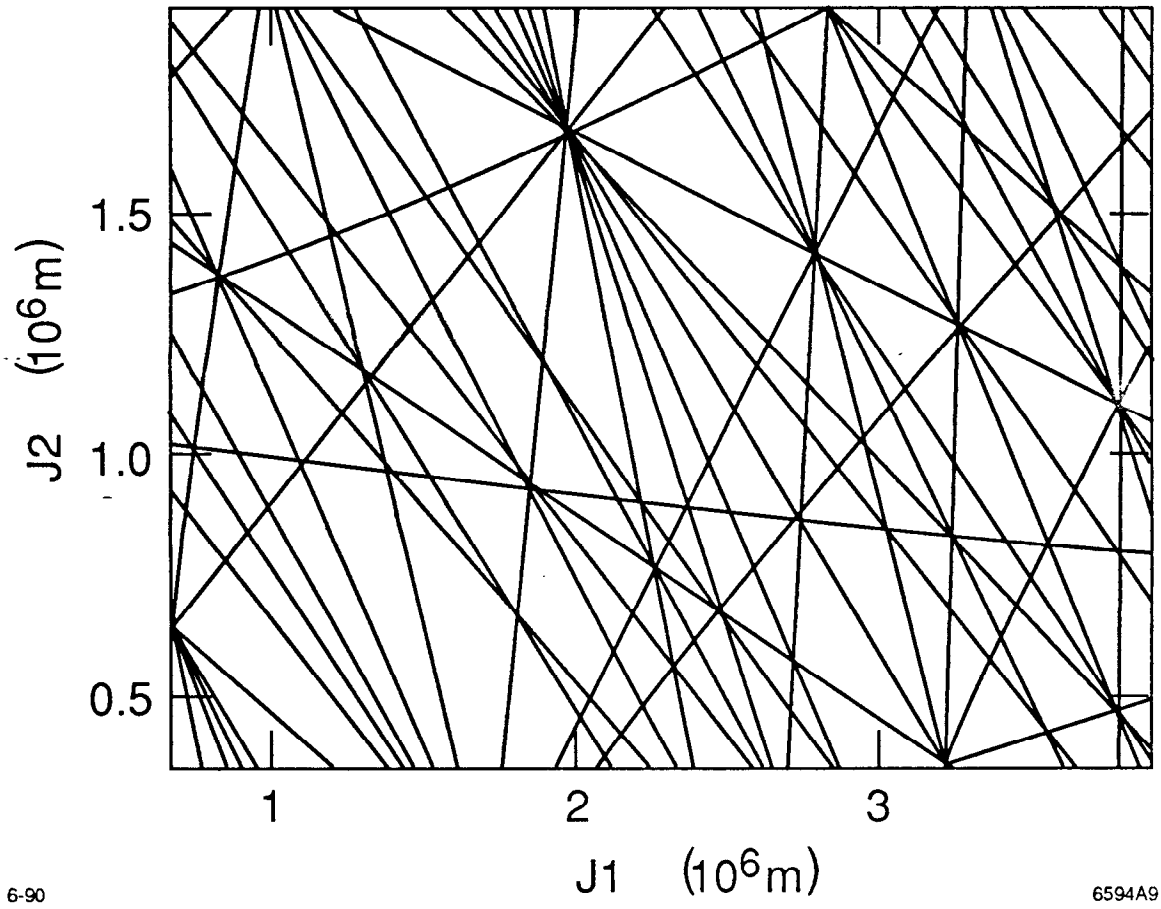

Fig. 9

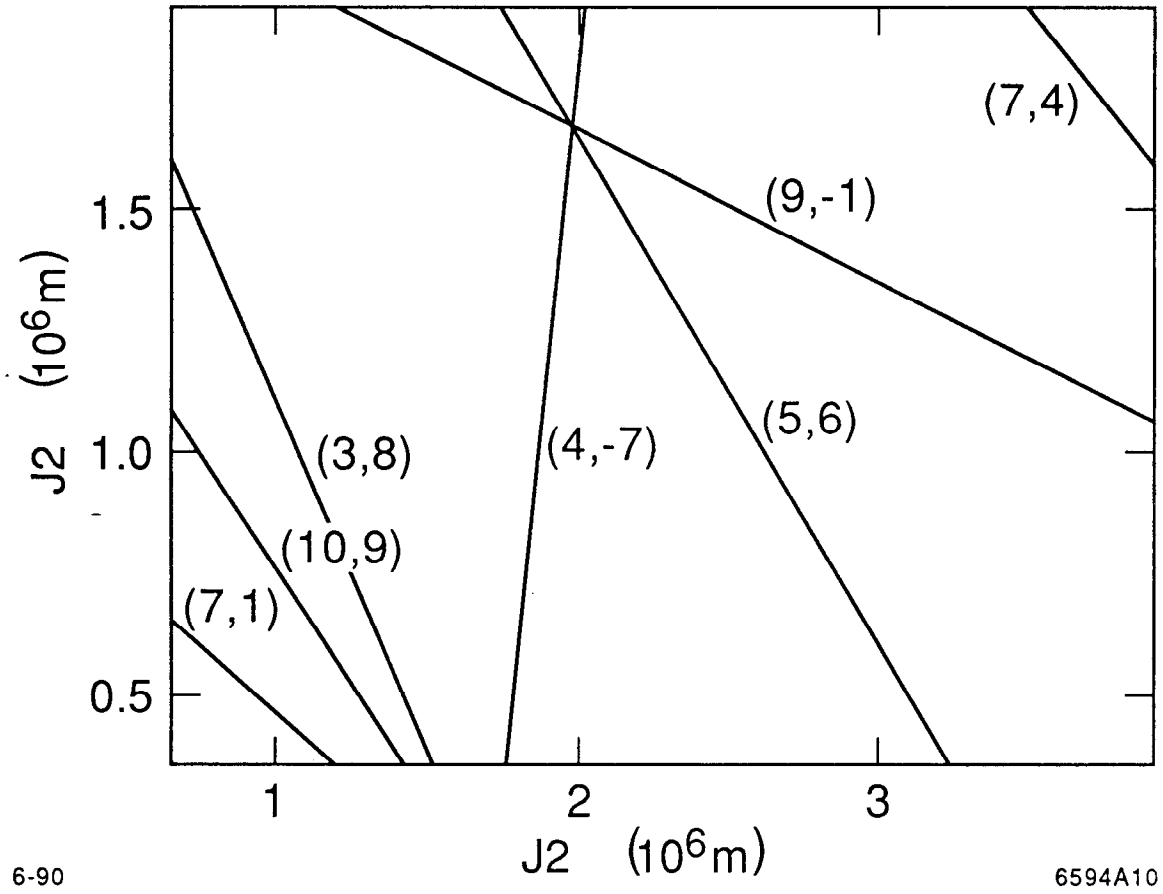

Fig. 10

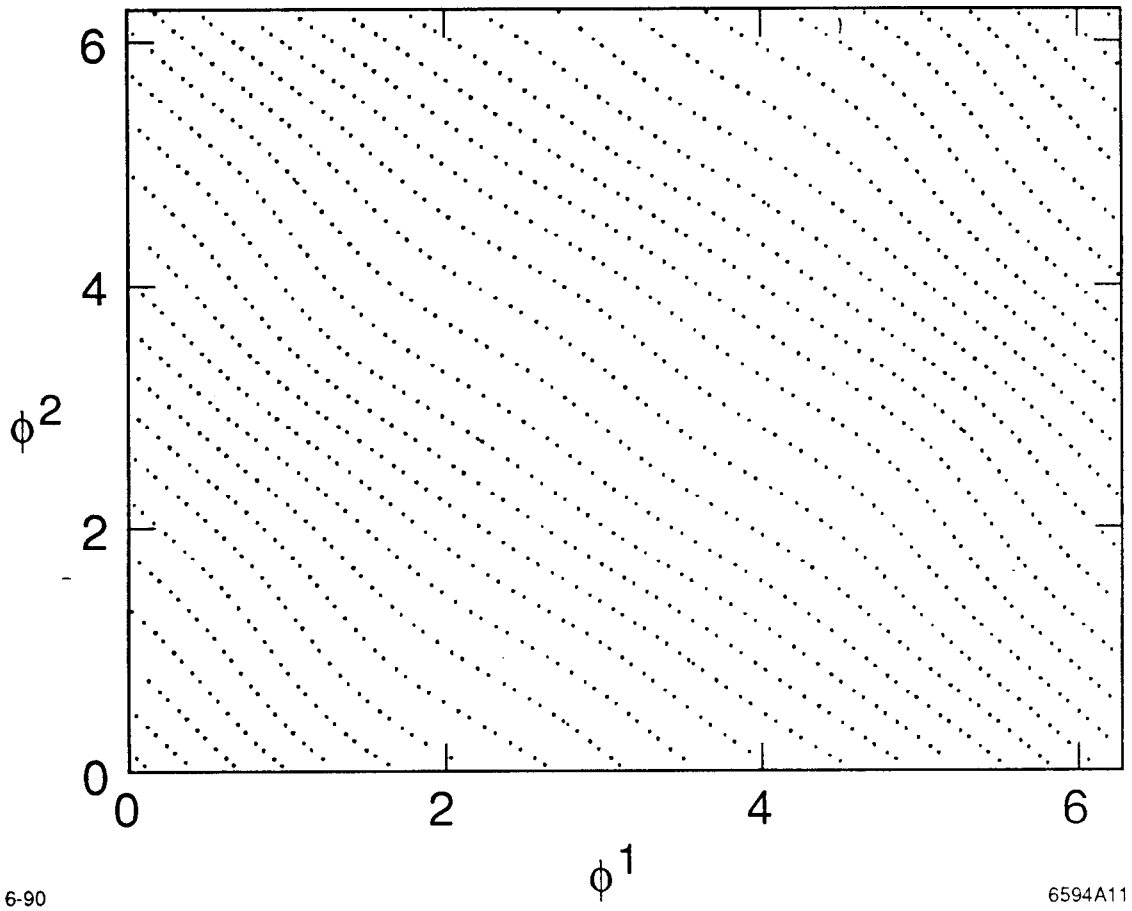

Fig. 11

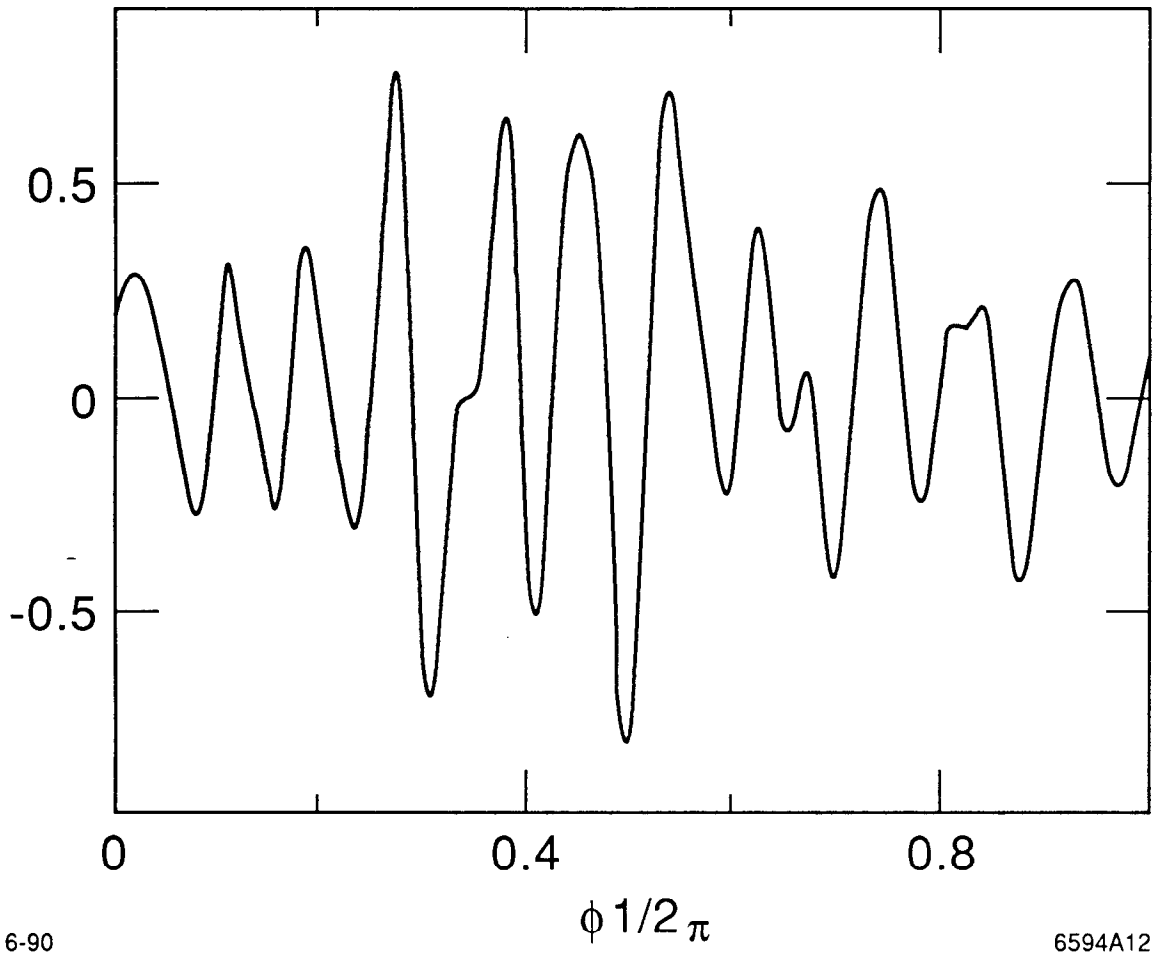

Fig. 12

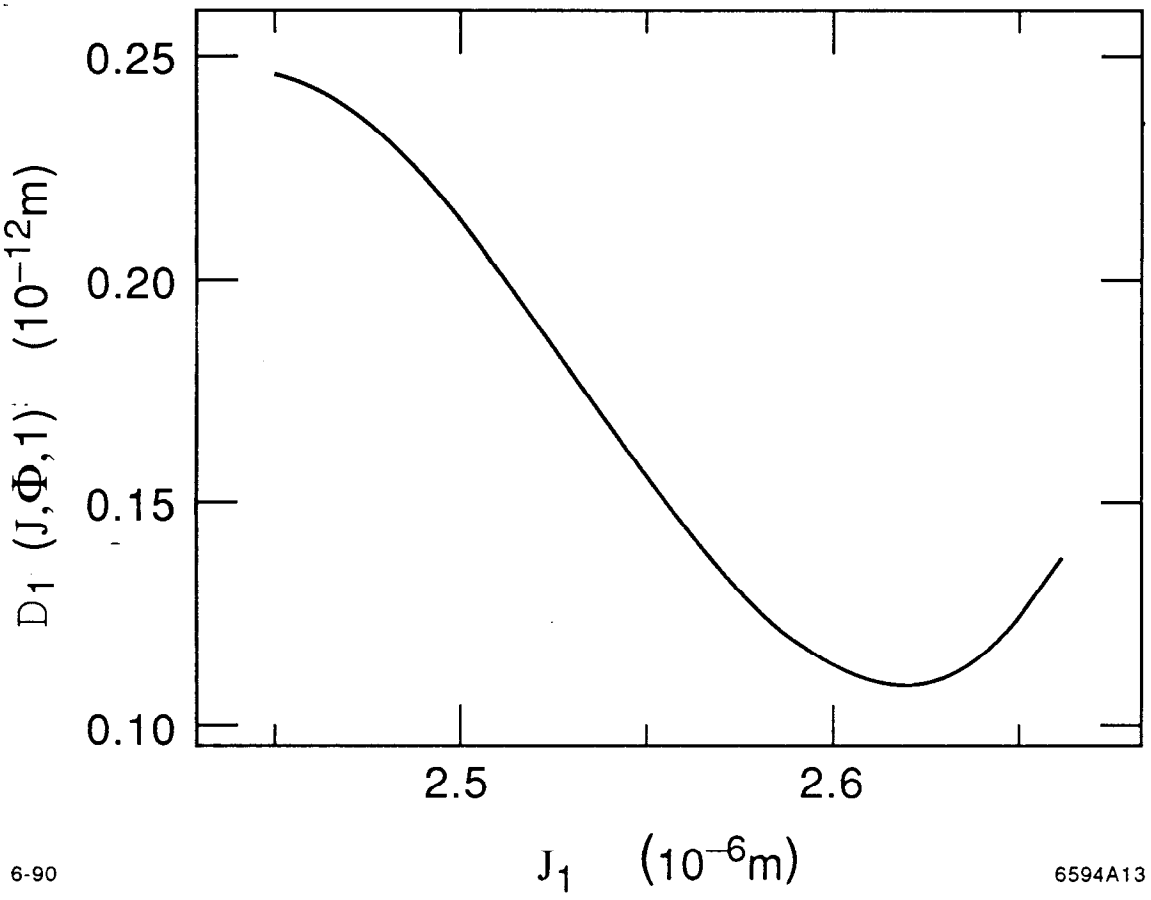

Fig. 13

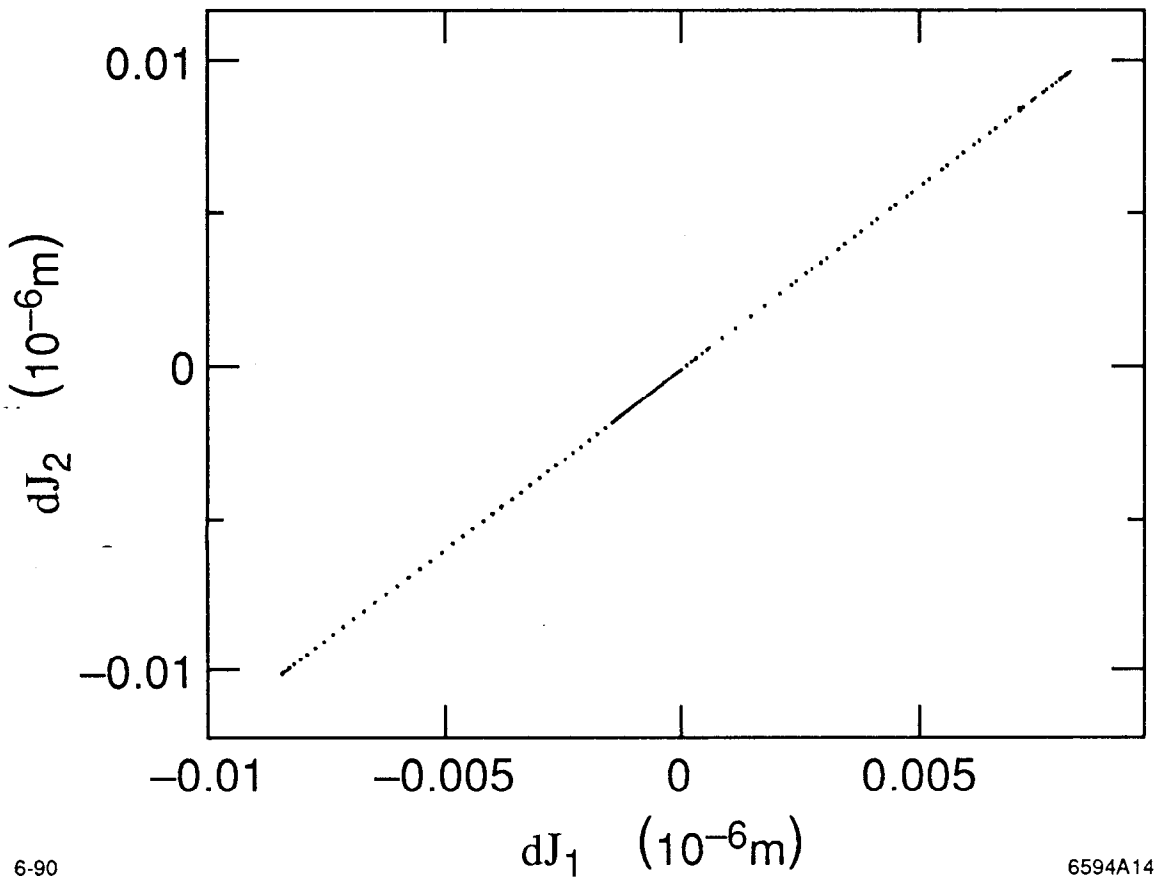

Fig. 14

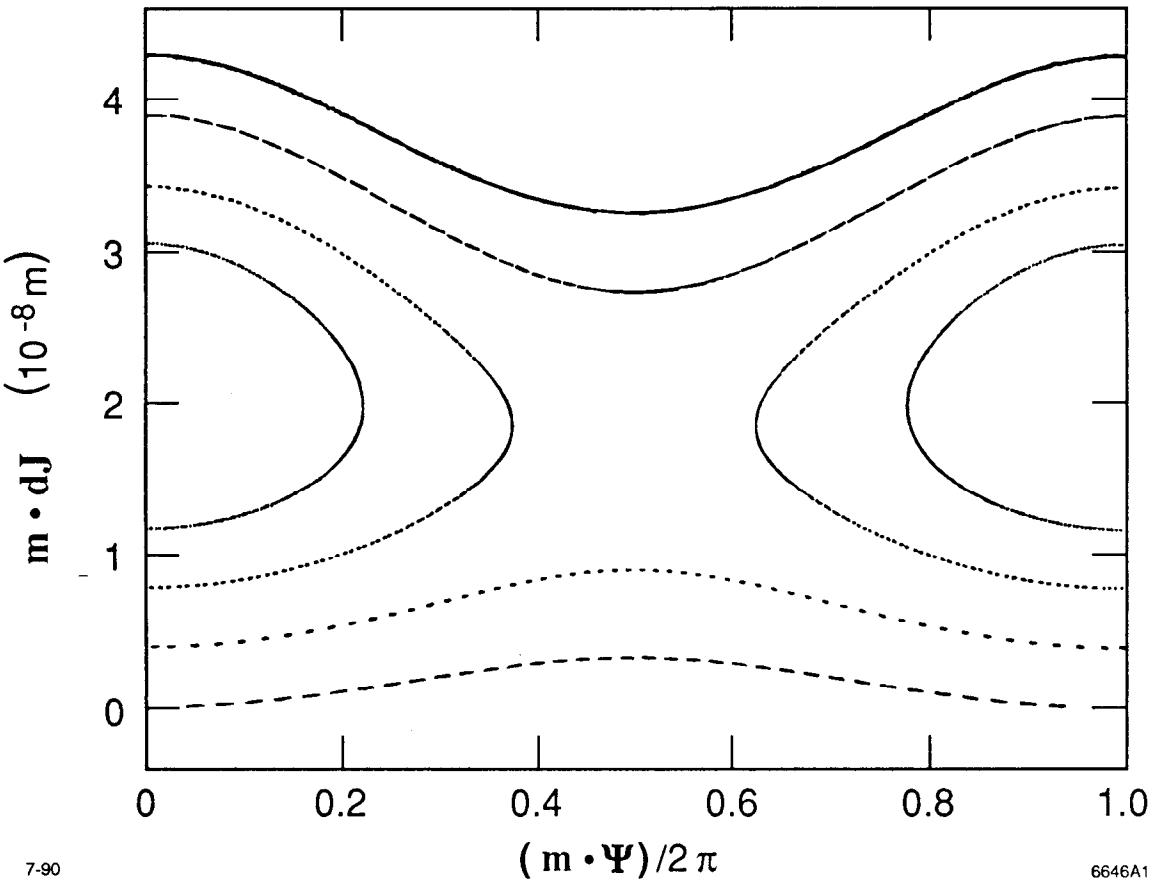

Fig. 15